High accuracy measurements of nanometer-scale distances between fluorophores at the single-molecule level

Stefan Niekamp[1], Jongmin Sung[1], Walter Huynh[1], Ronald D. Vale[1]*, Nico Stuurman[1]

[1] Department of Cellular and Molecular Pharmacology and Howard Hughes Medical Institute, University of California, San Francisco, 600 16th Street, San Francisco, CA 94158.

* Corresponding author: ron.vale@ucsf.edu

Abstract

Measuring dynamics and distance changes of macromolecules provides insight into how molecular machines function. While single-molecule methods for measuring distances between two different colored fluorophores have been reported, we discovered that they become significantly error-prone below 20 nm, which is the size regime of most proteins. Here, we describe three methods that incorporate information about measurement and imaging errors to achieve facile measurements of distances between two distinct fluorophores with ~1 nm accuracy. To ensure high throughput and consistent measurements, we implemented all analysis tools as a μManager-plugin. To validate our methods, we determined the head-to-head distance of rigor-bound homodimeric kinesin-1 and the end-to-end distance of a coiled-coil of known length. We also applied these methods to a sample of unknown length, a domain of the dynein adaptor protein Bicaudal-D, and demonstrated conformational heterogeneity. In summary, these new methods allow high accuracy distance measurements of single-molecules with commonly used fluorescence microscopes and open source software.

INTRODUCTION

Understanding the spatial arrangement of biological macromolecules is crucial for discerning molecular mechanisms. While three-dimensional structures provide insight into the mechanism of a protein, the static state alone is often insufficient to understand how macromolecular machines perform their actions. By labeling single-molecules or complexes at defined sites with fluorescent dyes, it is possible to obtain static or dynamic distance measurements that provide information on conformational changes or molecular interactions. A widely used method for obtaining such distance information is single-molecule Förster resonance energy transfer (smFRET)[1]. However, smFRET is usually limited to a narrow range (typically 2-8 nm) and the calculation of absolute distances is influenced by the orientations of the fluorophores[2], which is often difficult to measure directly.

Direct distance measurement of single-molecules can now be made by super-resolution fluorescence imaging. A variety of super-resolution measurements have been implemented that separate distinct fluorophores by wavelength[3–5], in time by taking advantage of sequential photobleaching[6,7], by stochastic switching of fluorescent probe emission[8,9], or by changing illumination patterns[10,11]. However, all of these methods face multiple challenges in measuring nanometer distances accurately. First, the positions of the fluorescent probes have to be determined[12–14] with high resolution. Second, if differently colored fluorescent probes are used, the localizations have to be accurately registered[3,4]. Finally, the Euclidean distance has to be calculated correctly[15], requiring careful consideration of all available information, including localization uncertainties of individual probes and registration errors.

Previously developed methods addressed some of these challenges and made remarkable progress. Single-molecule high resolution colocalization (SHREC)[4,15] resolves nanometer distances by accounting for localization errors when measuring the separation between two chromatically different fluorophores. Pertsinidis et al.[3] developed a feedback-controlled system that enabled distance measurements with subnanometer precision and Mortensen et al.[5] reported ~1 nm resolution by imaging the same single-molecules multiple times.

However, distance measurements with nanometer accuracy and precision are not routine. Accounting for imaging errors is essential and slight imperfections have been shown to result in

systematic offsets of tens of nanometers[3,5,15]. Moreover, many of the currently existing methods do not allow for high throughput measurements across the entire field of view. In addition, widespread application of single-molecule nanometer distance measurements is hampered by the lack of available software tools, the requirement for complicated optical setups[3] and, most importantly, the inaccuracy of current methods when the true distance and localization errors are of similar size.

Here, we report new methods for circumventing the above limitations that are capable of routinely measuring two-color distances with ~1 nm accuracy. We implemented a new image registration routine based on a piecewise affine transformation[16] that yields registration errors of < 1 nm over the entire field of view on a standard total internal reflection fluorescence (TIRF) microscope. We also show that existing analysis methods like those of Churchman et al.[15] (which performs a fit to distance data with an asymmetric, two-dimensional probability distribution function), inaccurately determine distances when the true distance and localization errors of the individual probes are of similar order, which is very common for distances of ~2-20 nm. By incorporating available information about localization errors into the fitting routine, we describe methods that allow greatly improved resolution and accuracy for distance measurements of individual particles as well as the investigation of conformational heterogeneity of biological samples. We validated these new methods by measuring the head-to-head distance (~8 nm) of rigor-bound kinesin and the length of a known coiled-coil domain (CC3) from the dynein adapter protein Bicaudal D2 (BICD2)[17] with subnanometer accuracy. In addition, we applied these methods to investigate the structural properties of the coiled-coil domain CC1 of BICD2[17], which we show can adopt multiple conformations, in contrast to its rigid-rod like state when bound to dynein/dynactin[18]. The methods described here should have broad application to two-color distances measurements at the nanometer scale using commercially available microscopes and open source μManager[19] software.

RESULTS

Theoretical considerations and method implementation

Obtaining the distance between two probes emitting at different wavelengths involves 1) localizing the individual probes, 2) correcting registration errors between the two images, and 3) calculating the distance. By fitting a point spread function (PSF) to the intensity distribution of a single fluorophore, its position can be determined with nanometer precision[20]. However, even if high precision measurements are obtained, this does not guarantee that the measurement is close to the true value. Therefore, high accuracy is needed and consideration of errors is essential[21,22]. The uncertainty of distance measurements of multiple particles (σ_d) is comprised of the registration error[3] (σ_{reg}), and the two localization errors[13,14,23] (σ_{loc_1}) and (σ_{loc_2}). For multiple measurements of either the same particle or of many different particles, the localization errors themselves follow a distribution ($\sigma_{\sigma(loc_1)}$, $\sigma_{\sigma(loc_2)}$) and also have to be considered. Assuming that all errors in a large population are uncorrelated and of stochastic nature, the distance uncertainty σ_d is

$$\sigma_d = \sqrt{\sigma_{reg}{}^2 + \sigma_{loc_1}{}^2 + \sigma_{loc_2}{}^2 + \sigma_{\sigma_{loc_1}}{}^2 + \sigma_{\sigma_{loc_2}}{}^2}. \quad (1)$$

We note this is only true for samples consisting of particles with uniform probe distances and that for heterogeneous samples an additional error term σ_{con} has to be added.

To obtain distance information, the Euclidean distance between two fluorescent spots is determined. While most distance distributions of two fluorescent probes are Gaussian distributed, distances on the scale of the localization error are not (**Fig. 1 a-c**) but rather are given by the following two-dimensional probability distribution (P2D)[15]

$$p_{2D}(r) = \left(\frac{r}{\sigma_d{}^2}\right) exp\left(-\frac{\mu^2+r^2}{2\sigma_d{}^2}\right) I_0\left(\frac{r\mu}{\sigma_d{}^2}\right) \quad (2)$$

in which r is the measured Euclidean distance, μ the calculated distance, σ_d the distance uncertainty, and I_0 the modified Bessel function of integer order zero. Churchman et al.[4,15] fit this distribution (P2D - Eq. 2) to Euclidean distance data by means of a maximum likelihood estimation (MLE) with two parameters (μ and σ_d). In this paper, we will refer to this method as "Churchman-P2D".

However, using both experimental data and Monte Carlo simulations, we found that for distances of similar size as the distance uncertainty, small changes in uncertainty result in large changes in estimated distance (**Fig. 1 d**). An approximation for $\sigma_d \geq \mu$, which is not uncommon for distances on the nanometer scale, shows that the probability distribution (P2D - Eq. 2) becomes independent of distance μ (**Supplementary Note 1**), resulting in faulty distance predictions.

To address and better understand this problem, we performed Monte Carlo simulations (**Supplementary Software**) in which we varied true distance between the two fluorophores (d), distance uncertainty (σ_d) with its parameters (Eq. 1), number of pairs observed (N), and number of frames (observations) per pair (F) (**Supplementary Fig. 1**). While analyzing the simulated data, we realized that the distance uncertainty σ_d not only gives rise to the non-Gaussian shape but also can be determined experimentally. With this in mind, we developed "Avg-Sigma-P2D" and "Sigma-P2D", methods that use the localization errors σ_{loc_1} and σ_{loc_2} and their standard deviations $\sigma_{\sigma(loc_1)}$ and $\sigma_{\sigma(loc_2)}$ (Eq. 1) of the fluorophores' intensity distributions. In Avg-Sigma-P2D, we determine the average localization errors of all dye pairs and use the value of σ_d as a fixed parameter in the probability distribution function (P2D - Eq. 2). For Sigma-P2D, we perform the MLE distance fit with a fixed σ_d on each dye pair separately. In general, by fixing σ_d in the probability distribution function (P2D - Eq. 2), the analysis becomes much more sensitive to small changes in distance μ.

To even further improve precision, multiple observations of the same particle can be made, for example in a time series (**Supplementary Fig. 1**). Inspired by diPOLE[5] we developed a third distance measurement technique, which we called "Vector-P2D". In this method, observations for the same fluorescent pair from multiple frames are combined by averaging distances in x and y separately. We then use these averages to calculate the Euclidean distance of individual particles. This leads to a more accurate distance prediction than the frame-by-frame Euclidean distance average because of an improved localization of both molecules prior to distance calculation (**Supplementary Fig. 2**). Finally, with the increased throughput of our method, a distance estimate for multiple particles is derived by fitting all particles' distances to the probability distribution function (P2D - Eq. 2) rather than determining an average (as in diPOLE[5], to which refer as "Vector").

Fitting Monte Carlo simulated data with a true distance of 10 nm and a distance uncertainty of 11 nm with Avg-Sigma-P2D, Sigma-P2D, and Vector-P2D shows that these methods can predict the true distance with subnanometer accuracy (**Fig. 1 e, f**). In contrast, Churchman-P2D and Vector methods as well as a simple Gaussian fit are off of the true values by as much as 10 nm.

Avg-Sigma-P2D, Sigma-P2D, and Vector-P2D are superior for nanometer distance measurements

Next, we carried out an in depth comparison of distance analysis methods over a wide parameter range. We again used Monte Carlo simulations (**Supplementary Software**) and generated ten data sets with all possible combinations of the true distance (10 nm, 20 nm, 40 nm), the distance uncertainty (Eq. 1) (3.5 nm, 7 nm, 10.5 nm, 14 nm, 17.5 nm, 21 nm), the number of frames (1, 5, 10, 15), and the number of pairs (100, 1,000, 10,000). We then calculated the average offset from the expected distance as a measure of accuracy for the following six methods: Gaussian fit (**Fig. 2 a**), Churchman-P2D[4] (**Fig. 2 b**), Avg-Sigma-P2D (**Fig. 2 c**), Sigma-P2D (**Fig. 2 d**), Vector[5] (**Fig. 2 e**), and Vector-P2D (**Fig. 2 f**). This analysis showed that Churchman-P2D often fails for cases where distances are of similar size as distance uncertainties and that using a Gaussian fit is worse than the probability distribution from Eq. 2. Overall, Sigma-P2D estimated distances for all simulated imaging conditions with subnanometer accuracy, except for cases with $\sigma_d \ll \mu$ where the calculation failed. In our simulations, this was the case for distances of > 20 nm and σ_d < 3.5 nm. Avg-Sigma-P2D performs almost equally well (**Supplementary Fig. 3**), but tends to underestimate the true distance if $\sigma_d \gg \mu$ by about 5-10% which still results in an accuracy of 1 to 2 nm and is significantly better than Churchman-P2D or a Gaussian fit which can be off of the true values by more than ten nanometers. Vector-P2D also achieves subnanometer accuracy but does not work for cases where only single frames were recorded because it is then identical to Churchman-P2D and therewith limited by the same constraints. All in all, Avg-Sigma-P2D, Sigma-P2D, and Vector-P2D achieve distance predictions with subnanometer accuracy where current methods are off by as much as 10 nm.

Experimental validation of predicted localization errors

Avg-Sigma-P2D and Sigma-P2D can only be used with experimental data if the fluorophores' localization errors can be determined with high accuracy, because imprecise predictions lead to incorrect distance estimates (**Fig. 1 d**). To test the available theoretical predictions of localization errors, we first imaged fluorescent probes that varied in number of fluorophores and determined intensities, backgrounds and widths using the MLE Gaussian fit[13]. Based on these measurements, we compared the localization errors given by the equations of Thompson et al.[14] and the MLEwG method described by Mortensen et al.[13] (**Supplementary Fig. 4**). Both equations yielded fairly similar values, with the MLEwG resulting in slightly higher localization errors, as reported previously[13,24].

We then investigated the standard deviation of localization errors ($\sigma_{\sigma(loc_1)}$, $\sigma_{\sigma(loc_2)}$) for fluorescent probes with single Cy3 and Cy5 dyes, probes with a cluster of up to ten Cy3 and Alexa 647 dyes, and of TetraSpeck beads. We found that localization errors follow a probability distribution (**Supplementary Fig. 5)** that depends amongst other things on the illumination pattern and the number of fluorophores per particle. Using Monte Carlo simulations, we noticed that if variances of localization errors are not taken into account when using Avg-Sigma-P2D, distance measurements are less accurate (**Supplementary Fig. 6**). Hence, we included the standard deviations of localization errors in each measurement that used the Avg-Sigma-P2D analysis (see Eq. 1).

Next, we measured localization errors at various radiant exposures and compared these to those predicted by equations. We measured the variations in probe position in a time-lapse sequence to determine the experimental localization error. We determined the localization error of each probe by averaging the variance of its pairwise distance with each of the other probes in the image over more than 120 frames. The error predicted by the MLEwG fit for a single probe was calculated from the average pairwise localization error of that probe with all other probes from the same dataset. Interestingly, the measured and predicted localization errors correlate well ($R^2 \geq 0.8$) at low radiant exposures **(Supplementary Fig. 7)** but poorly for two of the three samples at high radiant exposures (**Supplementary Fig. 7 h, i**). We discovered that the poor correlation was caused by intersample distance changes during the measurements at a scale that dominated localization errors only at high radiant exposures (**Supplementary Fig.**

7, Supplementary Note 2). Taken together, the localization errors predicted by the MLEwG method described by Mortensen et al.[13] match the experimentally measured values well.

Registration error in the subnanometer range

For accurate two-color distance measurements by fluorescence microscopy, the localizations of the two colors have to be registered. To achieve this objective, multicolor fiducial markers, such as TetraSpeck beads, are imaged in both channels and a registration function to correct for the offset is calculated in silico. Most previously used registration methods either use a second-degree polynomial fit[25] or linear mapping functions[3]. However, these methods correct poorly for commonly observed distortions at the nanometer scale that are likely caused by optical imperfections outside of the optical components' tolerances[3,5]. We overcame these distortions by taking advantage of a two-step affine based registration procedure[16]. First, we performed a global affine transformation to bring single spots (imaged on two different cameras) in proximity for automated pair assignment, and then applied a piecewise affine transformation, correcting spot positions locally by only using nearby fiducial points (**Supplementary Fig. 8**). To ensure high quality of the registration map during the experiment, we determined the target registration error (TRE), which reports the distance (ideally 0) for fiducials other than the points used to create the registration map[26] and which is more critical than the fiducial registration error (FRE) (**Supplementary Fig. 9**).

We always acquired three data sets for every distance measurement in the following order (**Fig. 3 a**): Fiducial markers (e.g. TetraSpeck beads) to create the registration map, sample of interest, and again TetraSpeck beads to test the stability of the registration. Subsequently, we calculated the deviation between the markers' x and y positions in the two channels after alignment. Their mean μ_x and μ_y are the registration error along the x-axis and y-axis, respectively. Therewith the registration error σ_{reg} is given by

$$\sigma_{reg} = \sqrt{\mu_x^2 + \mu_y^2}. \tag{3}$$

To find the optimal parameter space for image registration we investigated various settings for the local piecewise affine transformation. Since piecewise affine alignment is based on a nearest neighbor search[16], three parameters can influence registration outcome: minimum and maximum number of fiducial points and the maximum distance to the control point. We varied

these parameters to test their impact on registration accuracy and precision. Overall, higher maximum distance and higher maximum number of points caused distortions indicating that the registration was not executed properly (**Supplementary Fig. 10**). On the other hand, when the maximum distance is too small, an area in the micrograph may not contain the minimum number of fiducials, and thus will not be corrected (white areas in **Supplementary Fig. 10 c**). More extensive analysis revealed that a minimum of 10 and maximum of 100 fiducial points and a maximum distance of 2 μm resulted in optimal channel registration (**Supplementary Fig. 11**) when a sufficient number of fiducial markers was acquired. This is approximately 10,000 markers for an 80 μm x 80 μm image. To obtain this number, ~ 400 images with ~ 25 beads per field of view were collected. All steps to create the affine and piecewise affine maps are implemented in a μManager plugin[19] (**Supplementary Protocol**). Using this approach, we routinely (76%) achieved registration accuracy σ_{reg} (Eq. 3) of < 1 nm (**Fig. 3 b-h**). We only analyze sample data when σ_{reg} was confirmed to be < 1 nm. We noticed that small changes in focus invalidated the mapping making an autofocus system essential. Moreover, we note that the registration precision (σ_x, σ_y) for TetraSpeck beads is higher than one would expect based on their localization errors and found that this is due to the problem that the color centers of TetraSpeck beads do not overlap and are shifted by a few nanometers as reported by others[5] (**Supplementary Note 3**). Taken together, piecewise affine alignment enables image registration at subnanometer accuracy over the entire field of view, even when using non-ideal fiducial markers.

Experimental validation shows nanometer accuracy and precision

To test Avg-Sigma-P2D, Sigma-P2D, and Vector-P2D experimentally, we imaged a kinesin-1 homodimer for which both heads were rigor-bound with the non-hydrolyzable nucleotide analogue AMP-PNP to adjacent tubulin dimers along a microtubule protofilament[27] (**Fig. 4 a**). The distance between the two motor domains is 8.2 nm (the tubulin dimer spacing). A cysteine-lite kinesin motor domain construct was used[27,28] and a single cysteine residue was introduced (E215C), which was reacted with an equimolar mixture of maleimide-Cy3 and maleimide-Cy5. Only motors that contained both Cy3 and Cy5 and that bound to a biotin-streptavidin immobilized and Alexa-488 labeled microtubule were selected for two-color distance measurements.

Results for the apparent head-to-head distance of the rigor-bound kinesins are shown in **Figure 4 b** and **c**. We analyzed the distance distribution using the same time-lapse series (containing 20 frames) both by treating each dye pair in each frame individually (**Fig. 4 b**) and by calculating the vector distance average for each dye pair (**Fig. 4 c**). Then, we fitted the data with the corresponding probability distributions and found that only Avg-Sigma-P2D (8.7 ± 0.9 nm), Sigma-P2D (8.5 ± 0.3 nm) and Vector-P2D (7.7 ± 1.2 nm) resulted in values close to the true distance of 8.2 nm. The error for the distance estimates was calculated by bootstrapping analysis. In contrast, the Gaussian fit, Churchman-P2D, and Vector estimated the distance as 13.2 ± 7.0 nm, 0.3 ± 1.0 nm, and 10.4 ± 5.0 nm, respectively. We note that the fit for Avg-Sigma-P2D and Sigma-P2D are almost identical but Sigma-P2D yields a higher precision. Moreover, it was important to select only microtubule-bound dual labeled particles, as unbound particles had larger distances throwing-off the probability distribution fits yielding incorrect results (**Supplementary Figure 15 a, b**). Since Avg-Sigma-P2D as well as Sigma-P2D fit the ensemble data well, we also concluded that Cy3-Cy5 distances vary little amongst the many kinesin particles analyzed and that the ensemble distance distribution is described well solely by localization errors and their variances. Moreover, Avg-Sigma-P2D fit well to the distance distribution of multiple time point images of individual particles (**Supplementary Figure 15 c-f**), indicating that the Cy3-Cy5 distance did not change during the experiment. Thus, by utilizing either Avg-Sigma-P2D, Sigma-P2D or Vector-P2D, we could determine the head-to-head of a kinesin dimer with nanometer accuracy and precision.

As an additional control, we imaged the coiled-coil domain CC3 of the dynein adapter protein Bicaudal D2 (BICD2)[17] for which the crystal structure has been solved[29] and has shown an end-to-end distance of 12 nm (**Fig. 5 a**). We fused an AviTag[30] and SNAP tag[31] to the N-terminus as well as a HALO tag[32] and AviTag to the C-terminus to enable labeling with fluorescent dyes and surface immobilization. Analyzing the distance distribution of BICD2 CC3 revealed that only the result for Vector-P2D (12.1 ± 1.2 nm) agreed with the predicted length whereas Avg-Sigma-P2D (18.7 ± 0.7 nm) did not fit the ensemble data well (**Fig. 5 c, e**, **Supplementary Fig. 16 a, b**). While Churchman-P2D seems to fit the data reasonably well, the error of the fit is large indicating the irreproducibility of the fitting approach (10.8 ± 4.3 nm). On the other hand, applying Avg-Sigma-P2D to individual particles resulted in a good agreement between fits and data (**Supplementary Fig. 16 c-e**). Since Avg-Sigma-P2D accounts for all localization errors and a registration error of approximately 1 nm can not explain the difference

between probability and distance distribution, our data shows that BICD2 CC3 particles vary in their color center distance. The observed heterogeneity is consistent with probe movement allowed by the flexible loops between BICD2 CC3 and the fluorescent tags (**Supplementary Fig. 16 f**). Taken together, Vector-P2D can measure the average distance of conformationally heterogeneous samples with nanometer accuracy.

Bicaudal D2 N-terminal fragment CC1 is not a rigid-rod

Next, we applied our methods to a sample without predetermined distance measurements. The BICD2 N-terminal coiled-coil domain CC1 forms a rigid-rod of ~32 nm length when bound in complex with dynein and dynactin[18], but it is not clear whether this is also true for unbound BICD2 CC1[33]. We therefore used Avg-Sigma-P2D, Sigma-P2D, and Vector-P2D to investigate its shape when bound to a microscope slide. Similar to the BICD2 CC3 domain, we added an Avi, HALO, and a SNAP tag to the construct (**Fig. 5 b**).

For BICD2 CC1, we measured an end-to-end distance of 16.7 ± 0.9 nm (**Fig. 5 f**, **Supplementary Fig. 17 a-c**) using Vector-P2D. This distance is much shorter than expected for a rigid rod (~32 nm)[33] but agrees with the predicted secondary structure of BICD2 CC1 (**Supplementary Fig. 18**), that consists of two coiled-coil domains - approximately 19 and 6 nm long - connected by an unstructured region (**Fig. 5 b**). As expected for a flexible sample, Avg-Sigma-P2D fit the ensemble data poorly since it does not account for sample heterogeneity (**Fig. 5 d**). Thus, our data shows that BICD2 CC1, when immobilized on a microscope slide, is on average only half as long as when bound to dynein/dynactin and thus BICD2 CC1 seems to bend in the unstructured region, allowing it to adopt a variety of conformations.

DISCUSSION

Here, we described two-color fluorescence microscopy procedures that routinely yield accurate distance measurements on the relevant length scale of most macromolecules (1-30 nm). Moreover, we show that this single-molecule procedure can uncover conformational heterogeneity of macromolecules. Thus, our method closes the gap between static, angstrom-level three-dimensional structure determination (e.g. X-ray and electron microscopy) and lower resolution observation of protein dynamics by light microscopy. We achieved this degree of accuracy by employing two-color fluorescence microscopy which was first reported more than 10 years ago[4,15]. However, we demonstrated that these earlier methods can lead to unreliable distance measurements below 20 nm.

Image Registration

Previous studies registering multi-color localizations with fiducial markers used polynomial fitting and achieved registration accuracy of ~3 nm[34]. By positioning the sample at a site corresponding to one specific camera pixel and by employing active positioning feedback of the stage as well as actively positioning the dichroic mirror splitting the emitted fluorescence, Pertsinidis et al.[3] achieved ~1 nm registration error. While very accurate, this method requires complex and costly instrumentation and operates with low throughput. We used a piecewise affine registration method that is commonly employed in other fields[16], but to our knowledge has not been used to align multi-color single-molecule images. Using ~10,000 fiducials covering a field of view of ~6,700 μm^2 we routinely achieved target registration errors < 1 nm over the entire field of view (**Fig. 3**). Our methods can be carried out with any standard TIRF microscope capable of single-molecule imaging, provided that alignment of the two channels is stable for the duration of the experiment (i.e. < 1 nm change in approximately 5-20 min). This requirement includes the necessity for a motorized stage, high quality autofocus system, and minimal sample movement during image exposure (i.e. < 1 nm sample movement for approximately 1 sec).

Distance calculations

Localization of each fluorescent molecule has an associated error that depends on the signal to noise ratio. At a flux of ~10,000 photons per image, which is typical for two-color distance measurements, localization errors are typically ~4 nm (**Supplementary Fig. 4**), which corresponds to a distance uncertainty of ~7 nm (Eq. 1). Thus, the distance uncertainty is similar to the scale of many macromolecules. It was previously shown that probe distances in a population of identical particles follow a probability density distribution (P2D - Eq. 2)[15]. However, fitting both distance and uncertainty yields incorrect results when the uncertainty and the distance are of similar size because localization errors dominate the fit of the equation (**Supplementary Note 1**).

To overcome this problem, we used information about localization uncertainties available from the fluorophore's MLE-Gaussian fit as a fixed parameter in Eq. 2. Hence, only the distance was fitted by the MLE, resulting in much more accurate distance estimations (Avg-Sigma-P2D and Sigma-P2D). Imaging individual particles for multiple frames and averaging their distance along x and y first and then calculating the Euclidian distance leads to better distance estimates than determining a frame-by-frame distance average. Combining the average distances from multiple particles using a fit with the probability distribution function in Eq. 2, enabled us to accurately determine average distances of samples with heterogeneous distances (Vector-P2D).

The three new distance measurement methods (Avg-Sigma-P2D, Sigma-P2D, Vector-P2D) presented in this work each have their own limitations and advantages. For samples that have a homogeneous distance distribution, Sigma-P2D will typically provide the most accurate results (**Fig. 2**). However, a distance estimation with Sigma-P2D can fail if the actual distance is about 10-fold larger than the distance uncertainty. In that case, Avg-Sigma-P2D or Vector-P2D (if more than five frames of the same dye pair were recorded) can be applied. For samples that have a heterogeneous distance distribution, Vector-P2D is the method of choice, because the other two methods will yield incorrect results since they only account for localization errors but not for sample heterogeneity. However, for Vector-P2D to work reliably, multiple frames have to be recorded (usually 5 or more). Thus, for a typical workflow, we recommend first applying Avg-Sigma-P2D to test for sample heterogeneity by evaluating the goodness of the fit to the distance distribution. We then would use either Sigma-P2D for homogeneous samples (good

agreement between Avg-Sigma-P2D fit and data) or Vector-P2D for heterogeneous samples (poor agreement between Avg-Sigma-P2D fit and data).

Using the open source μManager[19] software and our "Localization Microscopy" plugin, it takes less than two hours to complete data acquisition, image registration and analysis of a typical data set.

Applications

We validated our methods by determining the head-to-head distance of rigor-bound kinesin and measured its distance with all three methods with subnanometer precision and accuracy (**Fig. 4**). In addition, we tested the new methods on the coiled-coil CC3 of BICD2 and found heterogeneity in probe distance, which was within a range that is is most likely explained by the flexibility of fluorescent tag attachment. However, even for this heterogenous sample, we could determine the end-to-end distance with nanometer accuracy using the Vector-P2D method (**Fig. 5**). These results also indicate that the SNAP and Halo tags used for labeling BICD2 CC3 allow for free rotation of the fluorescent dyes, which is important for correct measurements[3].

Applying our methods to various samples that are typically used as "standards", we found a surprising heterogeneity in probe distance. This included a 30 bp dsDNA construct (~10 nm) labeled with Cy3 and Cy5[4] (**Supplementary Note 4, Supplementary Fig. 19**). In this case, we suspect that the heterogeneity is likely caused by hydrophobic or stacking effects of the fluorescent probes[3,5,21,22]. Heterogeneity in distances were also observed in DNA origamis with color centers at defined distances; in this case, the heterogeneity may arise from incomplete labeling and/or photobleaching of the multiple dye molecules used for each color. Even multi-colored TetraSpeck beads revealed color centers that were slightly displaced from one another, which might be due to non-uniformities arising in their production. Thus, while our methods faithfully and accurately measure two-color distances, the interpretation of the data requires caution with regard to probe environment and distribution.

We also measured the end-to-end distance of BICD2 CC1, for which a rigid-rod like shape was observed by cryo-electron microscopy when bound to dynein/dynactin[18] but for which the end-to-end distance in an unbound state is unknown. Our methods revealed that unbound

Bicaudal D2 CC1 is only half as long as predicted by a rigid-rod and that its length distribution is heterogeneous (**Fig. 5**). This increased flexibility in the unbound state may be necessary for autoregulation and could play a role in regulating dynein/dynactin binding and activation.

In addition to measuring distances and investigating conformational heterogeneity of biological macromolecules, the methods presented in this work can also be applied to characterize dynamic changes in protein conformation. Thus, our methodology is readily applicable to study biophysical properties of motor proteins such as dyneins, kinesins, and myosins and potential conformational changes of protein. With the improved resolution of these techniques, we expect that the mechanism of molecular machines with even smaller step sizes like ribosomes and chromatin remodelers can now be observed by fluorescence microscopy.

Finally, the theoretical concepts and their application to nanometer distance measurements presented in this work are not limited to two-color fluorescence microscopy but apply to all super-resolution imaging techniques[35]. As these methods venture into the regime of nanometer resolution[36], we anticipate that our methodology and open source software will be useful for a broad range of super-resolution fluorescence microscopy.

ACKNOWLEDGEMENTS

We thank A. Jain for critical discussions about the method. We are grateful to E. Jonsson for the kinesin plasmids and discussions about the kinesin distance measurements. The authors acknowledge funding from the National Institutes of Health (R37GM038499, R35GM118106 S.N., W.H., R.D.V., and N.S.; 1F32GM113366-01, J.S.) and the Howard Hughes Medical Institute.

AUTHOR CONTRIBUTIONS

S.N., J.S., R.D.V., and N.S. designed the research; N.S. and S.N. developed the software; S.N. and J.S. performed Monte Carlo simulations; S.N. and W.H. prepared samples; S.N. collected data; S.N., J.S., and N.S. analyzed the data; S.N., J.S., R.D.V., and N.S. wrote and edited the article; All authors read and commented on the paper.

COMPETING FINANCIAL INTEREST

R.D.V. and N.S. have a financial interest in Open Imaging, Inc., a company that provides support for the μManager software used in this manuscript.

METHODS

Flow-cell preparation. We made custom, three-cell flow chambers using laser-cut double-sided adhesive sheets (Soles2dance, 9474-08x12 - 3M 9474LE 300LSE), glass slides (Thermo Fisher Scientific, 12-550-123), and coverslips (Zeiss, 474030-9000-000). The coverslips were cleaned in a 5% v/v solution of Hellmanex III (Sigma, Z805939-1EA) at 50°C overnight and washed extensively with Milli-Q water afterwards. Finally, flow-cells were assembled so that each chamber holds ~ 10 µl (**Supplementary Fig. 8**).

Fluorescent beads for image registration. We used TetraSpeck beads (Thermo Fisher Scientific, T7279) with a diameter of ~100 nm for image registration. Samples for imaging are prepared according to the following protocol. We added 10 µl of 1 mg/ml Poly-D-lysine (Sigma, P6407) in Milli-Q water to the flow-cell and incubated for 3 min. Afterwards we washed with 20 µl of BRB80 (80 mM Pipes (pH 6.8), 1 mM EGTA, and 1 mM $MgCl_2$) and then added 10 µl of 1:1000 diluted Tetraspeck beads in BRB80 and incubated for 5 min. Finally, we washed the flow-cell with 40 µl of BRB80.

Preparation of dsDNA samples.

We purchased

strand A: /5Cy3/GGGTATGGAGATTTTTAGCGGAGTGACAGC/3Cy5Sp/

and strand B: /5BiosG/GCTGTCACTCCGCTAAAAATCTCCATACCC/3Bio/

for the 30 bp dual biotin dsDNA construct[4] from Integrated DNA Technologies. For the 30 bp single biotin dsDNA construct we swapped strand A for

strand C: /5BiosG/AAAAAAAAAAAAGCTGTCACTCCGCTAAAAATCTCCATACCC.

The double stranded constructs were assembled by mixing 10 µM of either strand A and B (dual biotin construct) or strand A and C (single biotin construct) with Assembly Buffer (20 mM Tris (pH 8.0), 1 mM EDTA, and 2.5 mM $MgCl_2$) and heating the mixture to 95°C for 5 min, followed by a cooling of 1°C per minute down to 20°C. For imaging, we diluted the constructs in Assembly Buffer to 3 pM. Samples for imaging are prepared according to the following protocol. First, we added 10 µl of 5 mg/ml Biotin-BSA (Thermo Fisher Scientific, 29130) in BRB80 to the flow-cell and incubated for 2 min. Then, we again added 10 µl of 5 mg/ml Biotin-BSA in BRB80 and incubated for 2 min. Afterwards we washed with 20 µl of BRB80. This was followed by addition of 10 µl of 0.5 mg/ml Streptavidin (Thermo Fisher Scientific,

S888) in PBS and a 2 min incubation. We then washed with 20 µl of BRB80. In a next step 10 µl of 3 pM dsDNA construct was added and incubated for 5 min. Next, we washed with 30 µl of BRB80 and finally added the PCA/PCD/Trolox oxygen scavenging system[37] in BRB80.

DNA-origami standards. Custom DNA origami nanorulers[38] were purchased from GATTAquant GmbH (Braunschweig, Germany). The nanoruler design is based on the 12HB and is externally labeled with fluorescent dye molecules (Cy3 and Alexa647). The 'center-of-mass' between the Cy3 binding sites and the Alexa647 binding sites is either 10 nm, 20 nm, or 40 nm. Each color has up to 10 binding sites with an expected labeling efficiency of 50-80%. In addition, each nanoruler has multiple biotins attached to allow for immobilization on a coverslip. Samples for imaging are prepared according to the following protocol. First, we added 10 µl of 5 mg/ml Biotin-BSA in BRB80 to the flow-cell and incubated for 2 min. Then, we again added 10 µl of 5 mg/ml Biotin-BSA in BRB80 and incubated for 2 min. Afterwards we washed with 20 µl of BRB80. This was followed by addition of 10 µl of 0.5 mg/ml Streptavidin in PBS and a 2 min incubation. We then washed with 20 µl of BRB80 supplemented with 10 mM $MgCl_2$. In a next step 10 µl of DNA-origami ruler was added and incubated for 5 min. Next, we washed with 30 µl of BRB80 supplemented with 10 mM $MgCl_2$ and finally added the PCA/PCD/Trolox oxygen scavenging system[37] in BRB80 supplemented with 10 mM $MgCl_2$.

Kinesin cloning, purification and labeling. The kinesin construct was cloned and purified as previously described[27,28]. Briefly, cysteine residues were induced into a 'cysteine-light' human ubiquitous kinesin-1 dimer that is 490 amino acids long (K490). The homodimeric E215C K490 contains a carboxy-terminal His_6 tag.
The plasmid was transfected and expressed in Agilent BL21(DE3). Cells were grown in LB at 37°C until growth reached 0.6 OD_{280} and expression was induced by addition of 1 mM IPTG and then grown overnight at 18°C. Cells were pelleted and harvested in lysis buffer (25 mM Pipes (pH 6.8), 2 mM $MgCl_2$, 250 mM NaCl, 20 mM imidazole, 2 mM TCEP, 5% sucrose), and lysed by the EmulsiFlex homogenizer (Avestin) in the presence of protease inhibitors. After a spin in a Sorvall SS-34 rotor for 30 min at 30,000 x g, the supernatant was loaded onto a Ni-NTA resin (QIAGEN, 30210) and washed with additional lysis buffer. Then the protein was eluted by adding 300 mM of imidazole to the lysis buffer. The elutions were dialyzed overnight in dialysis buffer (25 mM Pipes (pH 6.8), 2 mM $MgCl_2$, 200 mM NaCl, 1 mM EGTA, 2 mM TCEP, 10% sucrose).

Afterwards, the E215C K490 was reacted for 4 h at 4°C with Cy3-maleimide (GE Healthcare, PA13131) and Cy5-maleimide (GE Healthcare, PA15131) at a motor/Cy3 dye/Cy5 dye ratio of 1:10:10. Unreacted maleimide dyes were quenched by the addition of 1 mM dithiothreitol (DTT). Subsequently the sample was purified by gel filtration over a S200 10/300GL column from GE Healthcare. Gel filtration buffer was composed of 25 mM Pipes (pH 6.8), 2 mM $MgCl_2$, 200 mM NaCl, 1 mM EGTA, 1 mM DTT, and 10% sucrose. Finally the sample was flash frozen and stored at -80°C.

Bicaudal D 2 cloning, purification and labeling. The mouse Bicaudal D 2 (BICD2) (GenBank accession no. AJ250106.1) CC1 (20-270aa) and the BICD2 CC3 (711-801aa) constructs containing Avi- and SNAP/Halo tags were cloned into a pMal-C2 vector digested downstream of the Factor Xa cleavage site using Gibson cloning. IDT gBlocks for CC1 and CC3 were used to fuse an AviTag[30] (GLNDIFEAQKIEWHE) followed by a GGS linker and SNAPf[31]-GGGS to the N-terminus of BICD2. The C-terminus contained a GGGS linker followed by Halotag[32]-GGS, the AviTag, and a GGS-His_6 sequence.
The plasmid was transformed into Agilent Bl21(DE3) cells for expression. An overnight culture was used to inoculate a 2L culture of LB. Cells were grown in the presence of antibiotics and 0.2% glucose to a density of 0.7 OD_{600} at 37°C. Expression was induced with 0.5mM IPTG and the cells were grown for another 18 h. Cells were harvested and pelleted at 6000 x g and then re-suspended in NiNTA lysis buffer (25 mM Hepes (pH 7.4), 200 mM NaCl, 20 mM imidazole, 5% glycerol) supplemented with 5 mM beta-mercaptoethanol and Roche protease inhibitor (EDTA-free) tablets (Sigma, 11873580001). Cells were then lysed using an Emulsiflex homogenizer (Avestin). The lysate was clarified using a Sorvall SS-34 rotor for 30 min at 30,000 x g and then incubated with 4 ml of amylose resin (NEB, E8021S) for 2.5 h rotating at 4°C. The beads were washed extensively using NiNTA lysis buffer and the bound protein was eluted with 10 ml of 10 mM maltose in lysis buffer. Afterwards 150 ul of 1 mg/ml Factor Xa (NEB, P8010S) was added to the eluted protein and incubated overnight to cleave off the MBP tag. In a next step 5 ml of 50% NiNTA beads were added to this solution and incubated for one hour at 4°C. Beads were washed extensively with NiNTA lysis buffer and then eluted with buffer containing an additional 250 mM imidazole. To this eluted sample, 1 ml of amylose was added and incubated for 1 hr at 4°C to bind any uncleaved protein still present. Then the solution was concentrated and injected onto a GE Healthcare Superose 6 10/300GL column. The gel filtration buffer (GF Buffer) contained 30 mM HEPES (pH 7.4), 150 mM NaCl, 10% glycerol, and

2 mM TCEP. Finally, peak fractions were pooled, concentrated, and flash frozen in liquid nitrogen.

Thawed protein was labeled overnight at 4°C with SNAP-Surface Alexa647 (NEB, S9136S) and Halo TMR (Promega, G8252) at a ratio of 8uM:20uM:20uM, respectively. The labeled protein was then put over a Zeba Spin Desalting Column with 7K MWCO (Thermo Fisher Scientific, 89882) to remove excess dye. An Avidity BirA-500 kit (Avidity, BirA500) was used to biotinylate the protein overnight at 4°C as per manufacturer instructions. The final labeled product was passed again through a Zeba spin column, and aliquots were flash frozen with liquid nitrogen and then stored at -80°C.

Preparation of microtubules. Tubulin was purified and polymerized as previously described[39]. Unlabeled tubulin, biotinylated tubulin, and fluorescent tubulin were mixed at a ratio of 8:2:1 in BRB80 and 1 mM GTP was added. Then the mixture was incubated in a 37°C water bath for 15 min. Afterwards 20 μM of Taxol (Sigma, T1912) was added and the mixture was incubated for an additional 2 h at 37°C. Before usage, microtubules were spun over a 25% sucrose cushion at ~160,000 *g* for 10 min in a tabletop centrifuge.

Preparation of flow-cells with kinesin. Flow-cells with immobilized kinesin were prepared as previously described[27]. First, we added 10 μl of 5 mg/ml Biotin-BSA in BRB80 to the flow-cell and incubated for 2 min. Then, we again added 10 μl of 5 mg/ml Biotin-BSA in BRB80 and incubated for 2 min. Afterwards we washed with 20 μl of BRB80 with 2 mg/ml β-casein (Sigma, C6905), 0.4 mg/ml κ-casein (Sigma, C0406). This was followed by addition of 10 μl of 0.5 mg/ml Streptavidin in PBS and a 2 min incubation. We then washed with 20 μl of BRB80 with 2 mg/ml β-casein, and 0.4 mg/ml κ-casein. In a next step 10 μl of polymerized Alexa488 labeled microtubules were added and incubated for 5 min. Next, we washed with 30 μl of BRB80 with 2 mg/ml β-casein, 0.4 mg/ml κ-casein, and 10 μM Taxol. Then, we added 10 μl of K490 in BRB80 with 2 mg/ml β-casein, 0.4 mg/ml κ-casein, 10 μM Taxol, and 1 mM AMP-PNP (Sigma, 10102547001) and incubated for 5 min. Afterwards we washed with 30 μl of BRB80 with 1 mg/ml β-casein, 0.2 mg/ml κ-casein, 10 μM Taxol, and 1 mM AMP-PNP. Finally we added the PCA/PCD/Trolox oxygen scavenging system[37] in BRB80 with 1 mg/ml β-casein, 0.2 mg/ml κ-casein, 10 μM Taxol, and 1 mM AMP-PNP.

Preparation of flow-cells with Bicaudal D 2. Samples for imaging are prepared according to the following protocol. First, we added 10 µl of 5 mg/ml Biotin-BSA in BRB80 to the flow-cell and incubated for 2 min. Then, we again added 10 µl of 5 mg/ml Biotin-BSA in BRB80 and incubated for 2 min. Afterwards we washed with 20 µl of BRB80. This was followed by addition of 10 µl of 0.5 mg/ml Streptavidin (Thermo Fisher Scientific, S888) in PBS and a 2 min incubation. We then again washed with 20 µl of BRB80. In a next step 10 µl of labeled BICD2 CC1 or CC3 construct was added and incubated for 5 min. Next, we washed with 30 µl of BRB80 and finally added the PCA/PCD/Trolox oxygen scavenging system[37] in BRB80.

Microscope setup. Every data collection was performed at room temperature (~23°C) using total internal reflection fluorescence (TIRF) inverse microscopy on a Nikon Eclipse Ti microscope equipped with a 100× (1.45 NA) oil objective (Nikon, Plan Apo λ). We used two stepping motor actuators (Sigma Koki, SGSP-25ACTR-B0) mounted on a KS stage (KS, Model KS-N) and a custom built cover to reduce noise by air and temperature fluctuations. A reflection based autofocus unit (FocusStat4) was custom adapted for our microscope (Focal Point Inc.). We applied Nikon Type NF2 immersion oil (Nikon, MXA22126) to all slides. Three laser lines at 488 nm (Coherent Sapphire 488 LP, 150 mW), 561 nm (Coherent Sapphire 561 LP, 150 mW), and 640 nm (Coherent CUBE 640-100C, 100 mW) were guided through an AOTF (Neos, 48062-XX-.55), enlarged 6 fold, passed through a quarter wave plate (ThorLabs, AQWP05M-600) and focused using an achromatic doublet f=100 mm on a conjugate back focal plane of the objective outside of the microscope. The TIRF angle was adjusted by moving this focusing lens. A TIRF cube containing excitation filter (Chroma, zet405/491/561/638x), dichroic mirror (zt405/488/561/638rpc), and emission filter (Chroma, zet405/491/561/647m) was mounted in the upper turret of the microscope. The lower turret contained a filter cube (Chroma, TE/Ti2000_Mounted, ET605/70m, T660lpxr, ET700/75m) that directs Cy3 emission towards the back camera and the Cy5 emission towards the left camera. We used two Andor iXon 512x512 EM cameras, DU-897E. The acquisition software was µManager[19] 2.0. All acquisitions were carried out with alternating excitation between the 561 and 640 laser lines (to avoid considerable back-ground fluorescence in the Cy5 channel caused by 561nm laser excitation). Image pixel size was 159 nm.

Data collection. For TetraSpeck bead acquisitions an exposure time of 100 msec and for all other samples 400 msec was used, if not otherwise specified. After every stage movement we

waited 1 sec before collecting data to minimize drift effects. We used the cameras in conventional CCD mode (i.e., no EM gain). All data sets were acquired with a '16 bit, conventional, 3000 MHz' setting and a preamp gain of 5x. More details of image acquisition settings and laser powers settings for each individual data set are shown in **Supplementary Table 4**. A step-by-step protocol for data acquisition is given in **Supplementary Protocol**.

Single-molecule localization. All emitters were fitted and localized using μManager's[19] 'Localization Microscopy' plug-in. For emitter fitting we implemented a Gaussian based maximum-likelihood estimation[13] in μManager[19] and used the following starting conditions. The x- and y-position were determined by centroid calculation, the width was set to 0.9 pixels, the background was calculated by summing the intensities of all outermost pixels of an ROI, and the intensity was determined by summing up all intensities within the ROI minus the background value. Subsequently, intensities and background were converted to photon count by applying the photon conversion factor and by correcting for camera offset as well as read noise (in CCD mode). Width as well as x- and y-coordinates were then converted from pixel to nanometer space (1 pixel = 159 nm). When fitting emitters with μManager's[19] 'Localization Microscopy' plug-in a noise threshold and box size can be set. Parameters for analysis are shown in **Supplementary Table 3**.
We then calculated the variance in fluorophore localization using the MLEwG method[13]. Note that we used intensity and background values determined by the aperture method[40] and not values determined by the MLE emitter fitting because the aperture method values agreed better with the experimentally measured variance (**Supplementary Figure 7**). A step-by-step protocol for single-molecule localization is given in **Supplementary Protocol**.

Image registration. For image registration two data sets were always acquired: Fiducial markers (Tetraspeck beads) to determine the registration map before imaging the sample of interest and beads to test the stability of the registration (TRE) after the sample of interest. The registration map is then calculated with beads from the first acquisition as follows: First, a global affine transformation is determined and second, a piecewise affine transformation[16] for local correction is calculated (**Supplementary Fig. 8**). Afterwards the TRE is determined by the deviation of channel one's position to channel two's position in x and y after alignment (Eq. 3). Settings for piecewise affine maps are a minimum of 10 and a maximum of 100 fiducial points as well as a maximum distance of 2 μm except for **Figure 3 g**, **h**, and **Supplementary Figure**

14 where a maximum distance of 3 µm was used, and in **Supplementary Figure 10** where values are provide in the figure caption. A step-by-step protocol for image registration is given in **Supplementary Protocol**.

Data analysis and distance determination. All data sets were analyzed using µManager's[19] 'Localization Microscopy' plug-in. The maximum-likelihood based fitting method (Gaussian fit, Churchman-P2D, Avg-Sigma-P2D, Sigma-P2D, Vector-P2D, and Vector) to calculate the distance between two fluorophores is either indicated in the figure and/or in the figure caption. Churchman-P2D[4] applies the probability distribution as shown in equation 2 with the calculated distance µ and the distance uncertainty σ_d as parameters. Avg-Sigma-P2D makes use of the same probability distribution as Churchman-P2D but determines the distance uncertainty σ_d from experimental data (Eq. 1) and only has the calculated distance µ as parameter. Sigma-P2D also uses experimental determined localization errors (as Avg-Sigma-P2D) but performs the MLE for each dye pair and frame separately. Vector-P2D and Vector are similar to Gaussian fit and Churchman-P2D, respectively, except that observations of the same fluorescent pair are subsequently combined by first averaging distances in x and y separately before calculating the Euclidean distance compared to the a frame-by-frame Euclidean distance average as used in Gaussian fit and Churchman-P2D. A standard error of the mean (S.E.M.) for distance calculations (**Figure 4** and **5**) was determined by means of bootstrapping. Parameters for analysis are shown in **Supplementary Table 3** and **5**. A step-by-step protocol for data analysis is given in **Supplementary Protocol**.

Monte Carlo simulations. *In silico* two-color distance measurements by means of Monte Carlo simulation were carried out with a custom Python script. In brief, the true distance µ, the two localization errors σ_{loc_1} and σ_{loc_2}, their underlying distributions ($\sigma_{\sigma(loc_1)}$, $\sigma_{\sigma(loc_2)}$), sample conformational heterogeneity σ_{con}, the number of pairs observed, and the number of frames (observations) per pair can be varied in parallel. The simulation for each parameter combination can be repeated multiple times if desired. For the variance in the fluorophores localization a Gaussian distribution is applied to true positions of channel 1 and 2 and a Gamma distribution is applied as the underlying distribution of the variance in the fluorophores localization for channel 1 and 2. For more details see **Supplementary Software**.

Statistics. For each result obtained, the inherent uncertainty due to random or systematic errors and their validation are discussed in the relevant sections of the manuscript. Details about the sample size, number of independent calculations, and the determination of error bars in plots are included in the figures and figure captions.

Code availability. The custom-written Python code for Monte Carlo simulations is available upon request. μManager acquisition and analysis software is available as **Supplementary Software** under the Berkeley Software Distribution (BSD) license and development is hosted on GitHub at https://github.com/micro-manager/micro-manager.

FIGURES

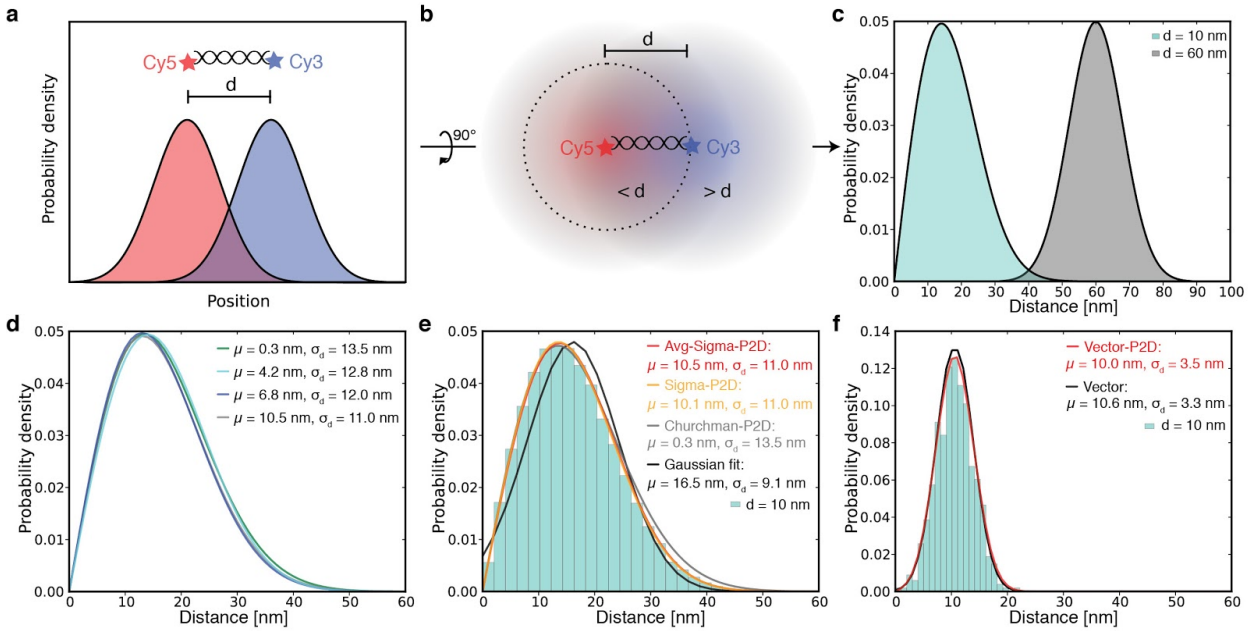

Figure 1 | Determination of nanometer distances from skewed distributions. (**a**) Side view of two gaussian distributed intensity profiles of a Cy3 and Cy5 molecule separated by a well defined true distance d. (**b**) Top view of the same fluorescence intensity distributions as shown in **a**. Circle with dotted line has a radius d around the position of the Cy5 molecule. Assuming the true position of Cy5 is known, each measurement that finds Cy3 inside the circle will be less than d away from Cy5 and measurements finding Cy3 outside the circle are more than d away from Cy5. Integrating the intensities of the blue molecule inside and outside the circle shows that the intensity outside the circle is higher than inside. Consequently, the probability for measuring distances larger than d is higher than measuring distances lower than d. Halos represent position / distance uncertainty. (**c**) Probability distributions for the case seen in **a** and **b** when the true distance d is of similar size or smaller than the distance uncertainty (turquoise) and when the distance is much larger than the distance uncertainty (gray). (**d**) Probability distribution (Eq. 2) plotted for various parameter combinations of calculated distance μ and distance uncertainty σ_d shows clearly that small variations in σ_d lead to large changes in estimation of μ. (**e**) Histogram of Monte Carlo simulated data with true distance d of 10.0 nm and a given distance uncertainty σ_d of 11.0 nm fitted with Avg-Sigma-P2D (red), Sigma-P2D (orange), Churchman-P2D (grey), and Gaussian fit (black). (**f**) Same data as in **e** but analyzed with Vector-P2D (red) and Vector (black). For Monte Carlo simulated data in **e** and **f**, the

simulation was carried out for 10,000 molecules with 10 observations each assuming perfect channel registration and uniform sample probe distances.

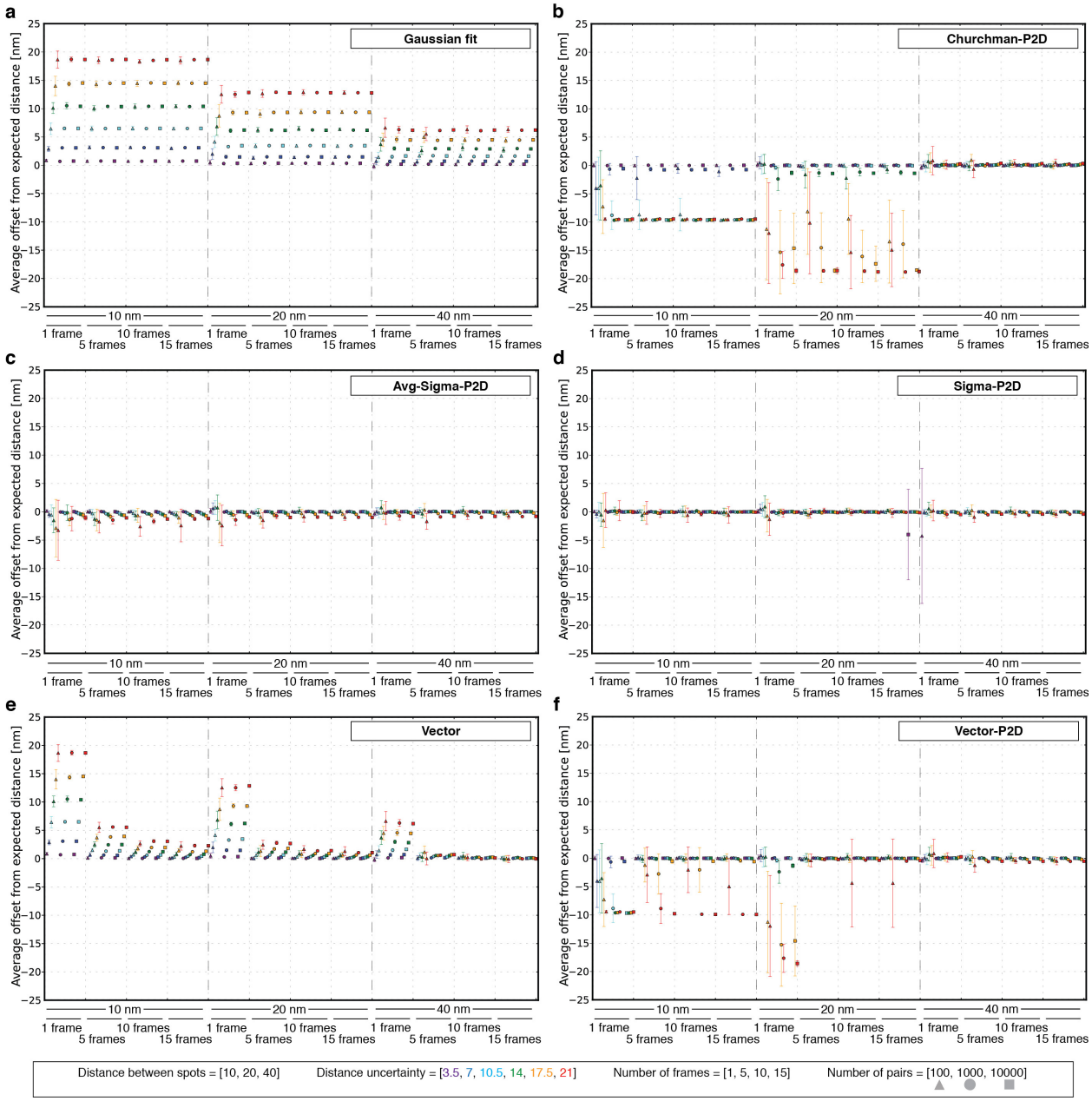

Figure 2 | Performance of distance prediction methods evaluated with Monte Carlo simulated data. Average offset from the expected distance was calculated based on 10 simulations for all possible combinations of the true distance (10 nm, 20 nm, 40 nm), the distance uncertainty (3.5 nm, 7 nm, 10.5 nm, 14 nm, 17.5 nm, 21 nm), the number of frames (1, 5, 10, 15), and the number of pairs (100, 1,000, 10,000). Results for fitting with (**a**) Gaussian fit, (**b**) Churchman-P2D, (**c**) Avg-Sigma-P2D, (**d**) Sigma-P2D, (**e**) Vector, and (**f**) Vector-P2D using the μManger[19] 'Localization Microscopy' plug-in. If fitting failed for more than 30% of the

simulations of one parameter combination, data point is not shown. Error bars in **a**-**f** show standard deviations of 10 independent simulations.

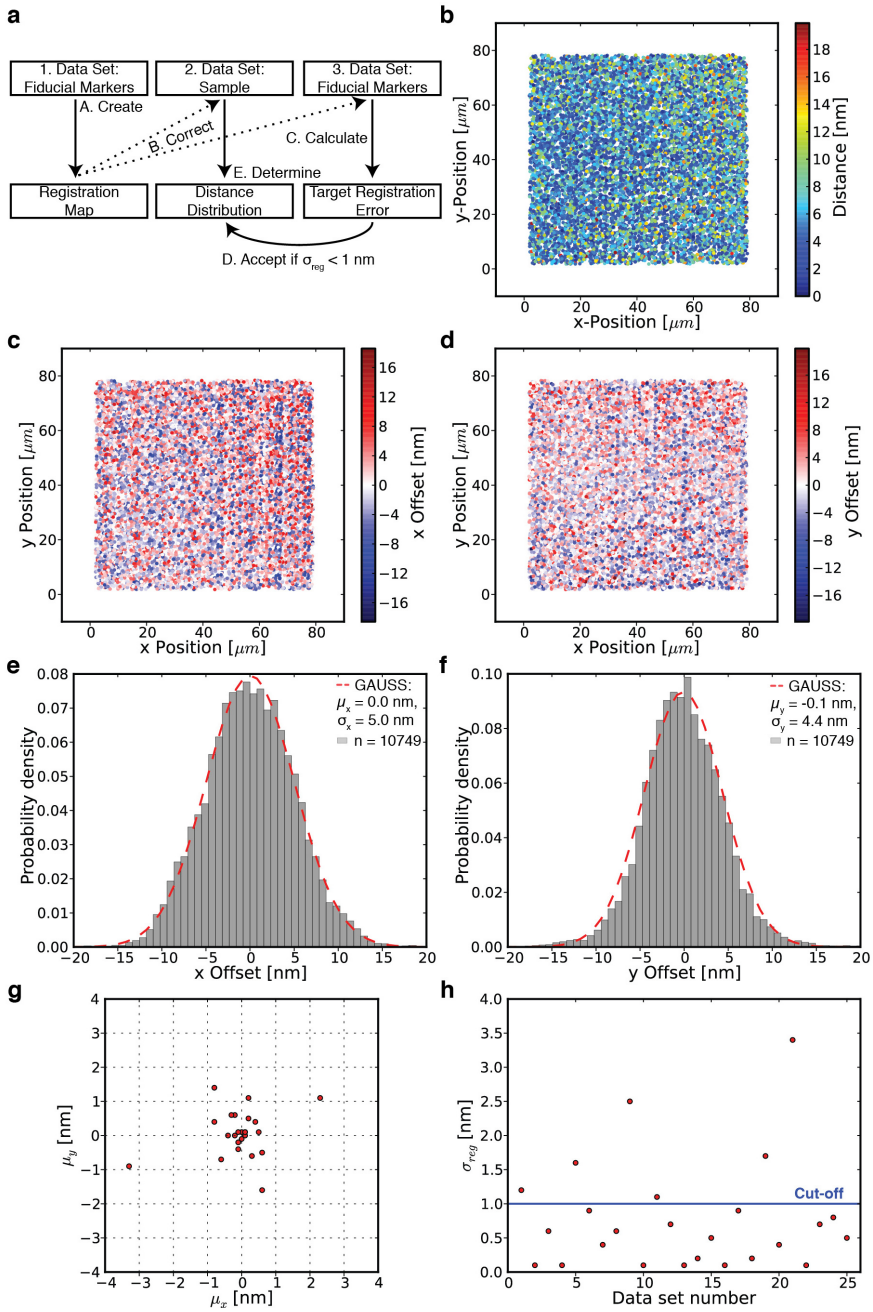

Figure 3 | Image registration workflow, accuracy, and reproducibility. (**a**) Workflow of image acquisition and registration process. (**b**) Euclidean distance after registration of fiducial markers other than the ones used to create the registration map (Target Registration Error - TRE). (**c**) Same data set as in **b** but the offset along the x-axis is shown. Negative values (blue dots) mean that channel 1 has a smaller number for its x position whereas positive values (red dots) represent fiducials where channel 2 has a smaller number for its x position. (**d**) Same as in **c** but along the y-axis. (**e**) Histogram of x-axis offset with Gaussian fit (dashed red line) of data shown

in **c**. (**f**) Histogram of y-axis offset with Gaussian fit (dashed red line) of data shown in **d**. (**g**) X-axis μ_x and y-axis μ_y component of registration error for 25 independent image registrations. (**h**) Same data as in **g**, but registration accuracy σ_{reg} (TRE) is shown for each of the 25 data sets. We accepted data sets for distance determination if $\sigma_{reg} < 1$nm (blue line cutoff). One frame per TetraSpeck bead was acquired. Details about fitting parameters in **Supplementary Table 3**.

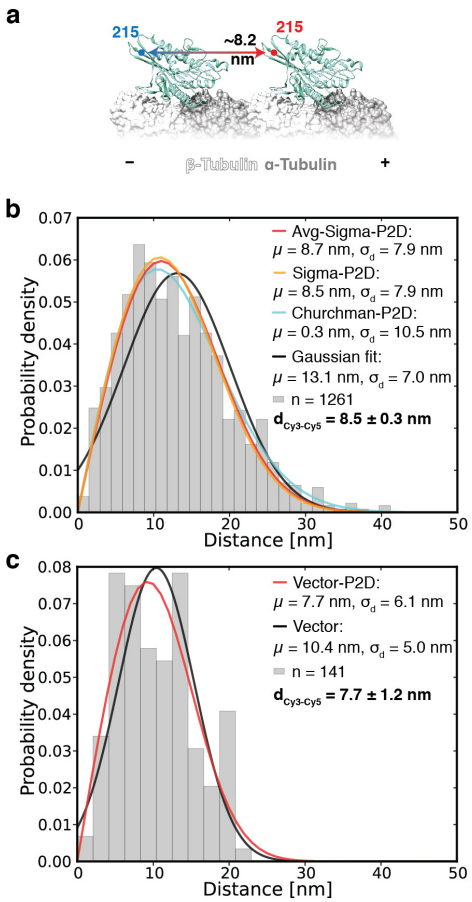

Figure 4 | Head-to-head distance of rigor-bound kinesin as measured by Avg-Sigma-P2D, Sigma-P2D, and Vector-P2D. (**a**) Diagram of two-head-bound kinesin on a microtubule based on crystal structure (PDB: 4LNU)[41] and created with UCSF Chimera[42]. Position of Cy3 and Cy5 dye are shown as blue and red dots, respectively. (**b**) Histogram of head-to-head distance measurements of rigor-bound kinesin fitted with Avg-Sigma-P2D (red), Sigma-P2D (orange), Churchman-P2D (cyan), and Gaussian fit (black). The standard deviation of the head-to-head distance ($d_{Cy3\text{-}Cy5}$) was calculated by bootstrapping analysis and is based on the Sigma-P2D fit. (**c**) Histogram of vector averaged head-to-head distance measurements of rigor-bound kinesin analyzed with Vector-P2D (red) and Vector (black). The standard deviation of the head-to-head distance ($d_{Cy3\text{-}Cy5}$) was calculated by bootstrapping analysis and is based on the Vector-P2D fit. Single-molecule distances in **b** and **c** were obtained by selecting time-lapse series of individual molecules (see **Supplementary Table 5**). Details about fitting parameters in **Supplementary Table 3**.

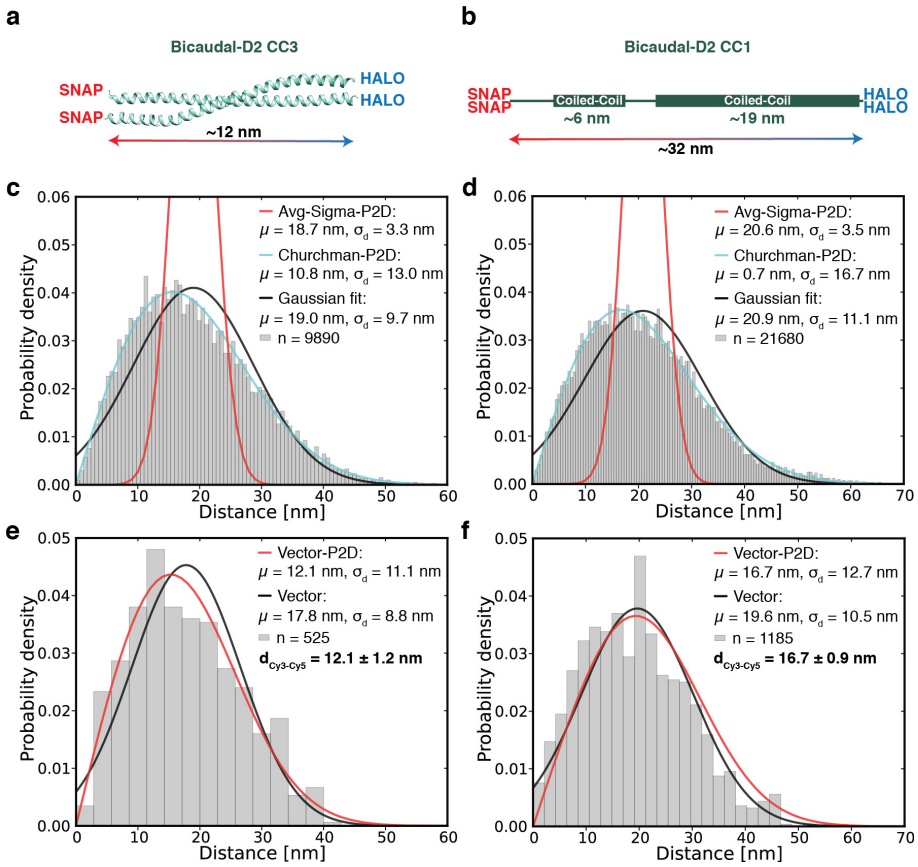

Figure 5 | End-to-end distance of Bicaudal D2 CC1 and CC3 as measured by Avg-Sigma-P2D and Vector-P2D. (**a**) Diagram of SNAP[31] and HALO[32] labeled Bicaudal D2 CC3 based on crystal structure (PDB: 4BL6)[29] and created with UCSF Chimera[42]. (**b**) Predicted domain structure of Bicaudal D2 CC1 based on estimations from the MPI Bioinformatics Toolkit[43]. (**c**) Histogram of end-to-end distance measurements of Bicaudal D2 CC3 fitted with Avg-Sigma-P2D (red), Churchman-P2D (cyan), and Gaussian fit (black). (**d**) Same as **c** but for Bicaudal D2 CC1. (**e**) Histogram of vector averaged end-to-end distance measurements of Bicaudal D2 CC3 analyzed with Vector-P2D (red) and Vector (black). The standard deviation of the end-to-end distance ($d_{Cy3\text{-}Cy5}$) was calculated by bootstrapping analysis and is based on the Vector-P2D fit. (**f**) Same as **e** but for Bicaudal D2 CC1. Single-molecule distances in **c-f** were obtained by selecting time-lapse series of individual molecules (see **Supplementary Table 5**). Details about fitting parameters in **Supplementary Table 3**.

REFERENCES

1. Roy, R., Hohng, S. & Ha, T. A practical guide to single-molecule FRET. *Nat. Methods* **5,** 507–516 (2008).
2. Ha, T. Single-molecule methods leap ahead. *Nat. Methods* **11,** 1015–1018 (2014).
3. Pertsinidis, A., Zhang, Y. & Chu, S. Subnanometre single-molecule localization, registration and distance measurements. *Nature* **466,** 647–651 (2010).
4. Churchman, L. S., Okten, Z., Rock, R. S., Dawson, J. F. & Spudich, J. A. Single molecule high-resolution colocalization of Cy3 and Cy5 attached to macromolecules measures intramolecular distances through time. *Proc. Natl. Acad. Sci. U. S. A.* **102,** 1419–1423 (2005).
5. Mortensen, K. I., Sung, J., Flyvbjerg, H. & Spudich, J. A. Optimized measurements of separations and angles between intra-molecular fluorescent markers. *Nat. Commun.* **6,** 8621 (2015).
6. Gordon, M. P., Ha, T. & Selvin, P. R. Single-molecule high-resolution imaging with photobleaching. *Proc. Natl. Acad. Sci. U. S. A.* **101,** 6462–6465 (2004).
7. Ram, S., Prabhat, P., Chao, J., Ward, E. S. & Ober, R. J. Resolution beyond Rayleigh's criterion: a modern resolution measure with applications to single molecule imaging. in *2007 IEEE Dallas Engineering in Medicine and Biology Workshop* 110–113 (2007).
8. Betzig, E. *et al.* Imaging intracellular fluorescent proteins at nanometer resolution. *Science* **313,** 1642–1645 (2006).
9. Rust, M. J., Bates, M. & Zhuang, X. Sub-diffraction-limit imaging by stochastic optical reconstruction microscopy (STORM). *Nat. Methods* **3,** 793–795 (2006).
10. Hell, S. W. & Wichmann, J. Breaking the diffraction resolution limit by stimulated emission:

stimulated-emission-depletion fluorescence microscopy. *Opt. Lett.* **19,** 780–782 (1994).

11. Gustafsson, M. G. L. Nonlinear structured-illumination microscopy: wide-field fluorescence imaging with theoretically unlimited resolution. *Proc. Natl. Acad. Sci. U. S. A.* **102,** 13081–13086 (2005).
12. Yildiz, A., Tomishige, M., Vale, R. D. & Selvin, P. R. Kinesin walks hand-over-hand. *Science* **303,** 676–678 (2004).
13. Mortensen, K. I., Churchman, L. S., Spudich, J. A. & Flyvbjerg, H. Optimized localization analysis for single-molecule tracking and super-resolution microscopy. *Nat. Methods* **7,** 377–381 (2010).
14. Thompson, R. E., Larson, D. R. & Webb, W. W. Precise nanometer localization analysis for individual fluorescent probes. *Biophys. J.* **82,** 2775–2783 (2002).
15. Churchman, L. S., Flyvbjerg, H. & Spudich, J. A. A non-Gaussian distribution quantifies distances measured with fluorescence localization techniques. *Biophys. J.* **90,** 668–671 (2006).
16. Pitiot, A., Malandain, G., Bardinet, E. & Thompson, P. M. Piecewise affine registration of biological images. in *WBIR* 91–101 (Springer, 2003).
17. Hoogenraad, C. C. & Akhmanova, A. Bicaudal D Family of Motor Adaptors: Linking Dynein Motility to Cargo Binding. *Trends Cell Biol.* **26,** 327–340 (2016).
18. Urnavicius, L. *et al.* The structure of the dynactin complex and its interaction with dynein. *Science* **347,** 1441–1446 (2015).
19. Edelstein, A., Amodaj, N., Hoover, K., Vale, R. & Stuurman, N. Computer control of microscopes using μManager. *Curr. Protoc. Mol. Biol.* **Chapter 14,** Unit14.20 (2010).
20. Yildiz, A. *et al.* Myosin V walks hand-over-hand: single fluorophore imaging with 1.5-nm localization. *Science* **300,** 2061–2065 (2003).

21. Enderlein, J., Toprak, E. & Selvin, P. R. Polarization effect on position accuracy of fluorophore localization. *Opt. Express* **14,** 8111–8120 (2006).

22. Stallinga, S. & Rieger, B. Accuracy of the gaussian point spread function model in 2D localization microscopy. *Opt. Express* **18,** 24461–24476 (2010).

23. Ober, R. J., Ram, S. & Ward, E. S. Localization accuracy in single-molecule microscopy. *Biophys. J.* **86,** 1185–1200 (2004).

24. Stallinga, S. & Rieger, B. The effect of background on localization uncertainty in single emitter imaging. in *2012 9th IEEE International Symposium on Biomedical Imaging (ISBI)* 988–991 (2012).

25. Goshtasby, A. Image registration by local approximation methods. *Image Vis. Comput.* **6,** 255–261 (1988).

26. Fitzpatrick, J. M. & West, J. B. The distribution of target registration error in rigid-body point-based registration. *IEEE Trans. Med. Imaging* **20,** 917–927 (2001).

27. Mori, T., Vale, R. D. & Tomishige, M. How kinesin waits between steps. *Nature* **450,** 750–754 (2007).

28. Tomishige, M., Stuurman, N. & Vale, R. D. Single-molecule observations of neck linker conformational changes in the kinesin motor protein. *Nat. Struct. Mol. Biol.* **13,** 887–894 (2006).

29. Liu, Y. *et al.* Bicaudal-D uses a parallel, homodimeric coiled coil with heterotypic registry to coordinate recruitment of cargos to dynein. *Genes Dev.* **27,** 1233–1246 (2013).

30. Cull, M. G. & Schatz, P. J. [26] Biotinylation of proteins in vivo and in vitro using small peptide tags. in *Methods in Enzymology* **326,** 430–440 (Academic Press, 2000).

31. Keppler, A. *et al.* A general method for the covalent labeling of fusion proteins with small molecules in vivo. *Nat. Biotechnol.* **21,** 86–89 (2003).

32. Los, G. V. *et al.* HaloTag: a novel protein labeling technology for cell imaging and protein analysis. *ACS Chem. Biol.* **3,** 373–382 (2008).

33. Stuurman, N. *et al.* Interactions between coiled-coil proteins: Drosophila lamin Dm0 binds to the bicaudal-D protein. *Eur. J. Cell Biol.* **78,** 278–287 (1999).

34. DeWitt, M. A., Chang, A. Y., Combs, P. A. & Yildiz, A. Cytoplasmic dynein moves through uncoordinated stepping of the AAA+ ring domains. *Science* **335,** 221–225 (2012).

35. Sahl, S. J., Hell, S. W. & Jakobs, S. Fluorescence nanoscopy in cell biology. *Nat. Rev. Mol. Cell Biol.* **18,** 685–701 (2017).

36. Balzarotti, F. *et al.* Nanometer resolution imaging and tracking of fluorescent molecules with minimal photon fluxes. *Science* **355,** 606–612 (2017).

37. Aitken, C. E., Marshall, R. A. & Puglisi, J. D. An oxygen scavenging system for improvement of dye stability in single-molecule fluorescence experiments. *Biophys. J.* **94,** 1826–1835 (2008).

38. Schmied, J. J. *et al.* DNA origami-based standards for quantitative fluorescence microscopy. *Nat. Protoc.* **9,** 1367–1391 (2014).

39. McKenney, R. J., Huynh, W., Tanenbaum, M. E., Bhabha, G. & Vale, R. D. Activation of cytoplasmic dynein motility by dynactin-cargo adapter complexes. *Science* **345,** 337–341 (2014).

40. Franke, C., Sauer, M. & van de Linde, S. Photometry unlocks 3D information from 2D localization microscopy data. *Nat. Methods* **14,** 41–44 (2017).

41. Cao, L. *et al.* The structure of apo-kinesin bound to tubulin links the nucleotide cycle to movement. *Nat. Commun.* **5,** 5364 (2014).

42. Pettersen, E. F. *et al.* UCSF Chimera—A visualization system for exploratory research and analysis. *J. Comput. Chem.* **25,** 1605–1612 (2004).

43. Alva, V., Nam, S.-Z., Söding, J. & Lupas, A. N. The MPI bioinformatics Toolkit as an integrative platform for advanced protein sequence and structure analysis. *Nucleic Acids Res.* **44,** W410–5 (2016).

Supplementary Information

High accuracy measurements of nanometer-scale distances between fluorophores at the single-molecule level

Stefan Niekamp, Jongmin Sung, Walter Huynh, Ronald D. Vale, Nico Stuurman

SUPPLEMENTARY FIGURES

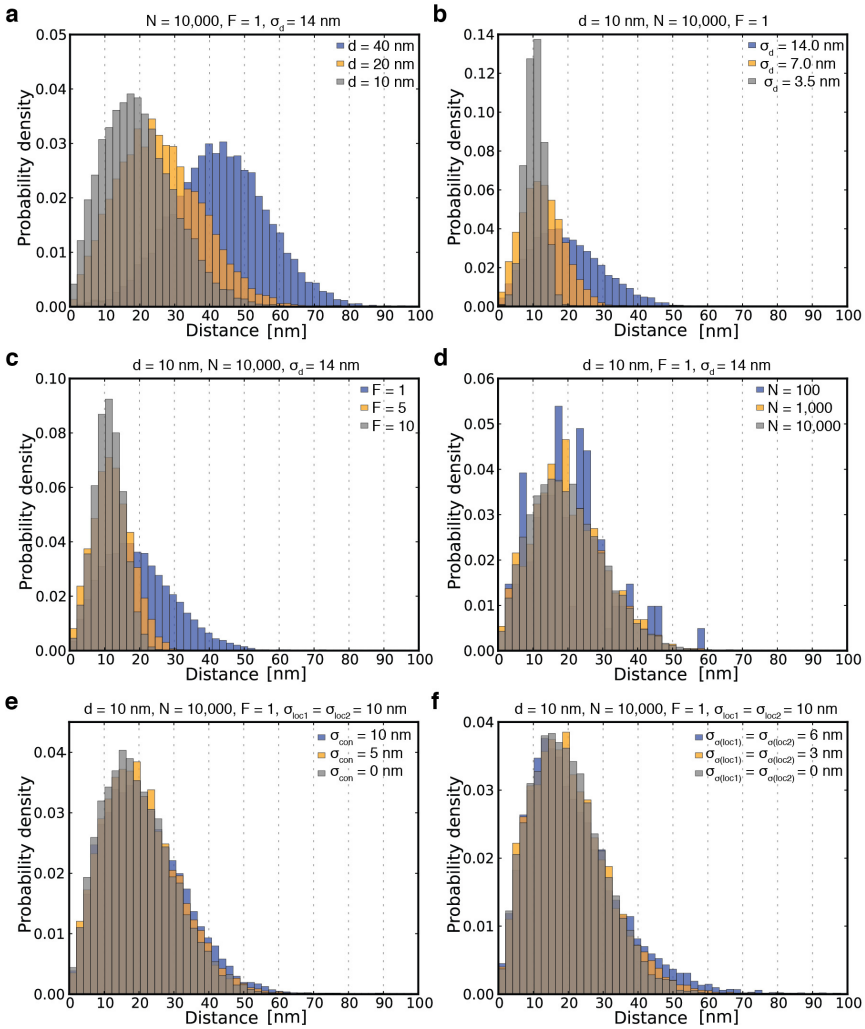

Supplementary Figure 1 | Monte Carlo simulated nanometer distance distributions for different conditions. (**a**) The true distance for a fluorophore pair of different color d is altered: 10 nm (gray), 20 nm (orange), and 40 nm (blue). (**b**) The distance uncertainty σ_d is modified: 3.5 nm (gray), 7.0 nm (orange), and 14.0 nm (blue). (**c**) The number of frames (observations) per pair F is changed: 10 (gray), 5 (orange), and 1 (blue) and if more than one frames was used, vector averaging is applied. (**d**) The number of pairs observed N is alternated: 10,000 (gray), 1,000 (orange), and 100 (blue). (**e**) The samples conformational heterogeneity σ_{con} underwent modifications (added as quadratic term in the square root term of σ_d in Eq. 1): 0 nm (gray), 5 nm (orange), and 10 nm (blue). (**f**) The standard deviation of the localization errors ($\sigma_{\sigma(loc_1)}$, $\sigma_{\sigma(loc_2)}$) is varied: 0 nm (gray), 3 nm (orange), and 6 nm (blue). If not specified otherwise, the standard parameters are d = 10 nm, σ_d = 14.0 nm, N = 10,000, F = 1 and σ_{con} = 0 nm.

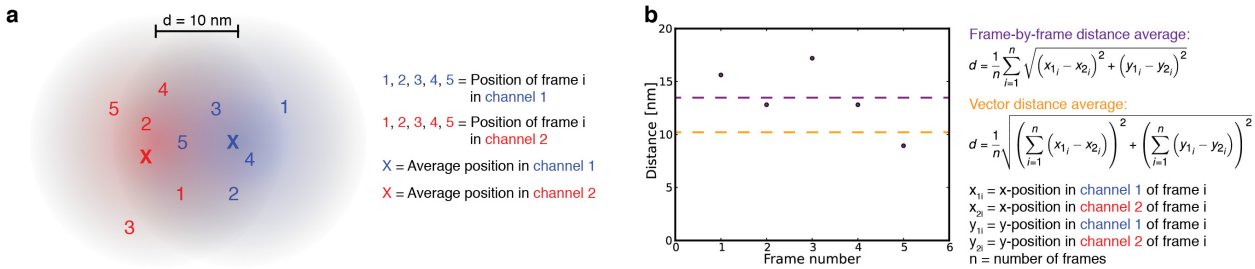

Supplementary Figure 2 | Frame-by-frame distance average calculation compared to vector distance average prediction. (**a**) Intensity distributions for two different fluorescent molecules in a red and a blue channel (as shown in **Fig. 1**) for a true distance of 10 nm. Five independent observations of both molecules were calculated by the means of Monte Carlo simulation (red and blue colored numbers 1 to 5, where '1' is the first and '5' is the last observation). 'X' represents the average position for each molecule after five frames. (**b**) Observed distance for a frame-by-frame distance measurement (purple dots) and its average (dashed purple line - 13.5 nm). Here the distance for each frame pair (1-1, 2-2, …) is determined and then an average is taken. Whereas for the vector average distance (dashed orange line - 10.1 nm) the average distance in x and y are calculated before the overall average distance is determined.

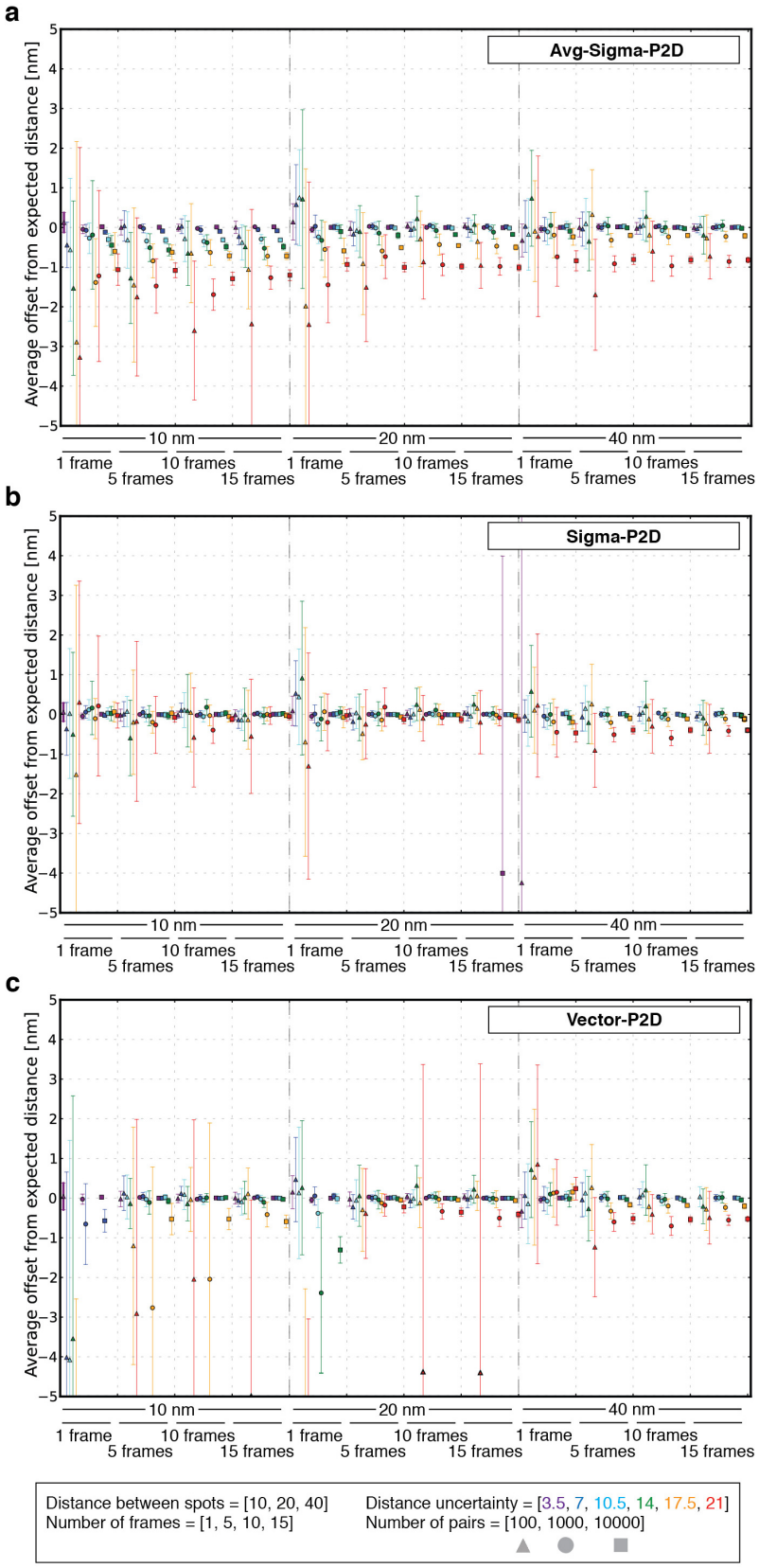
a
Avg-Sigma-P2D
Average offset from expected distance [nm]
5
4
3
2
1
0
−1
−2
−3
−4
−5
10 nm
20 nm
40 nm
1 frame
5 frames
10 frames
15 frames
b
Sigma-P2D
c
Vector-P2D
Distance between spots = [10, 20, 40]
Number of frames = [1, 5, 10, 15]
Distance uncertainty = [3.5, 7, 10.5, 14, 17.5, 21]
Number of pairs = [100, 1000, 10000]

Supplementary Figure 3 | Performance of Avg-Sigma-P2D, Sigma-P2D, and Vector-P2D evaluated with Monte Carlo simulated data. This is a magnified version of **Figure 2**. Average offset from the expected distance was calculated based on 10 simulations for all possible combinations of the true distance (10 nm, 20 nm, 40 nm), the distance uncertainty (3.5 nm, 7 nm, 10.5 nm, 14 nm, 17.5 nm, 21 nm), the number of frames (1, 5, 10, 15), and the number of pairs (100, 1,000, 10,000). Results for fitting with (**a**) Avg-Sigma-P2D, (**b**) Sigma-P2D, and (**c**) Vector-P2D using the μManger[1] 'Localization Microscopy' plug-in. If fitting failed for more than 30% of the simulations of one parameter combination, data point is not shown. Error bars in **a**-**c** show standard deviations of 10 independent simulations.

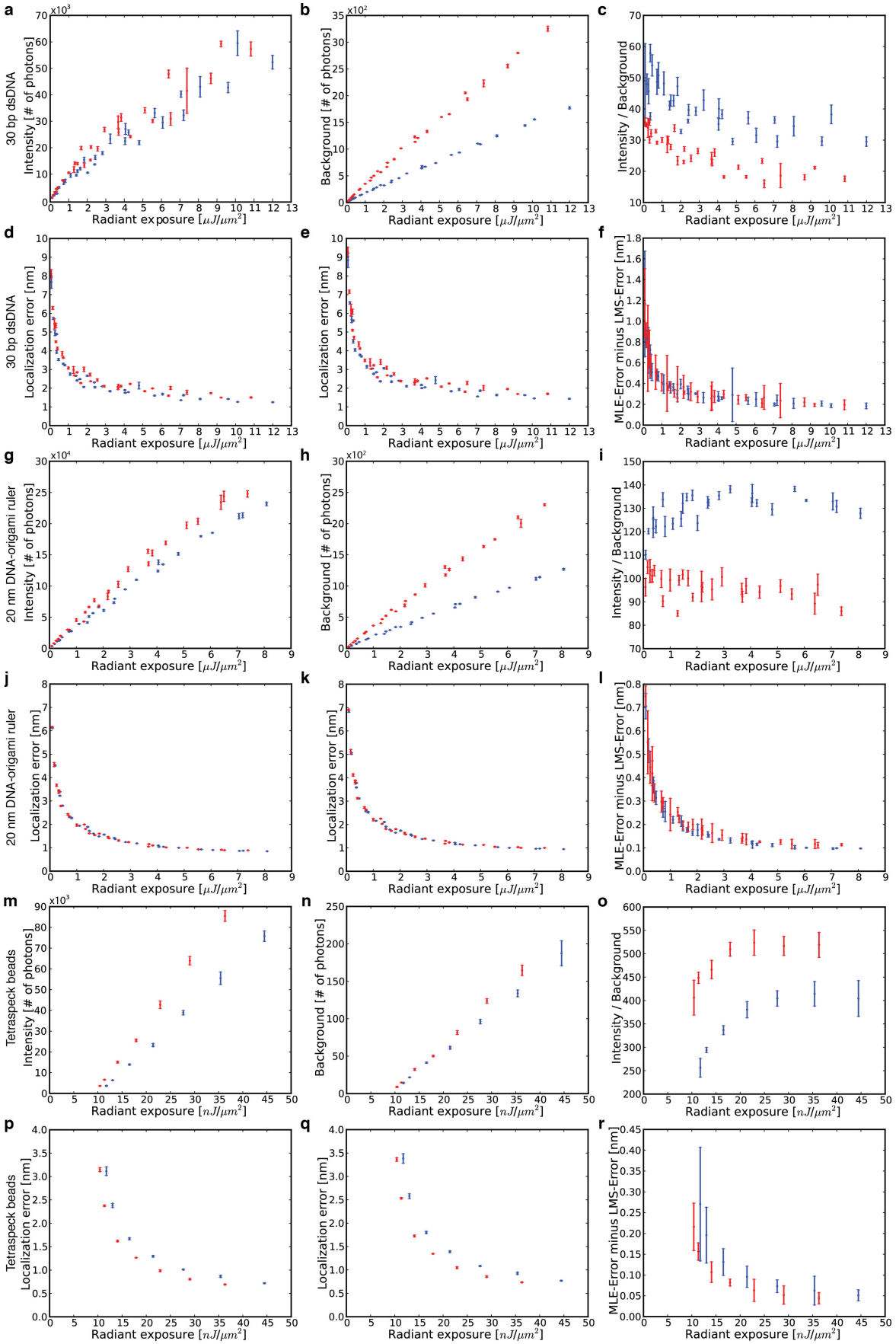
a
30 bp dsDNA
Intensity [# of photons]
x10^3
Radiant exposure [μJ/μm²]
b
Background [# of photons]
x10^2
Radiant exposure [μJ/μm²]
c
Intensity / Background
Radiant exposure [μJ/μm²]
d
30 bp dsDNA
Localization error [nm]
Radiant exposure [μJ/μm²]
e
Localization error [nm]
Radiant exposure [μJ/μm²]
f
MLE-Error minus LMS-Error [nm]
Radiant exposure [μJ/μm²]
g
20 nm DNA-origami ruler
Intensity [# of photons]
x10^4
Radiant exposure [μJ/μm²]
h
Background [# of photons]
x10^2
Radiant exposure [μJ/μm²]
i
Intensity / Background
Radiant exposure [μJ/μm²]
j
20 nm DNA-origami ruler
Localization error [nm]
Radiant exposure [μJ/μm²]
k
Localization error [nm]
Radiant exposure [μJ/μm²]
l
MLE-Error minus LMS-Error [nm]
Radiant exposure [μJ/μm²]
m
Tetraspeck beads
Intensity [# of photons]
x10^3
Radiant exposure [nJ/μm²]
n
Background [# of photons]
Radiant exposure [nJ/μm²]
o
Intensity / Background
Radiant exposure [nJ/μm²]
p
Tetraspeck beads
Localization error [nm]
Radiant exposure [nJ/μm²]
q
Localization error [nm]
Radiant exposure [nJ/μm²]
r
MLE-Error minus LMS-Error [nm]
Radiant exposure [nJ/μm²]

Supplementary Figure 4 | Evaluation of photophysical properties of three different probes in two channels. Quantification of 30 bp dsDNA constructs with a Cy3 dye on one and a Cy5 dye on the other end (**a-f**), of 20 nm DNA-origami nanorulers with 5-10 dyes of Cy3 and 5-10 dyes of Alexa 647 whose center of mass is 20 nm apart (**g-l**), and of TetraSpeck beads (**m-r**). Blue dots show values for channel 1 (Cy3 or Cy3 like dye(s)) and red dots for channel 2 (Cy5 or Cy5 like dye(s)). (**a**, **g**, **m**) Intensity in number of photons as a function of radiant exposure (**Supplementary Table 1**). (**b**, **h**, **n**) Background in number of photons as a function of radiant exposure. (**c**, **i**, **o**) Intensity over background ratio as a function of radiant exposure. (**d**, **j**, **p**) Localization error calculated with the equation from Thompson et al.[2] (Least Mean Squared (LMS)-Error) as a function of radiant exposure. (**e**, **k**, **q**) Localization error calculated with the MLEwG equation from Mortensen et al.[3] (MLE-error) as a function of radiant exposure. (**f**, **l**, **r**) Difference between LMS- and MLE-error as a function of radiant exposure. Error bars in **a**, **b**, **d**, **e**, **g**, **h**, **j**, **k**, **m**, **n**, **p**, and **q** show standard deviation of five repeats (new microscopy slides with fresh sample). Each repeat consists of at least 100 molecules and one frame was taken per molecule. For **c**, **f**, **i**, **l**, **o**, and **r** the error bar is calculated based on error propagation (linear addition). Details about fitting parameters in **Supplementary Table 3**.

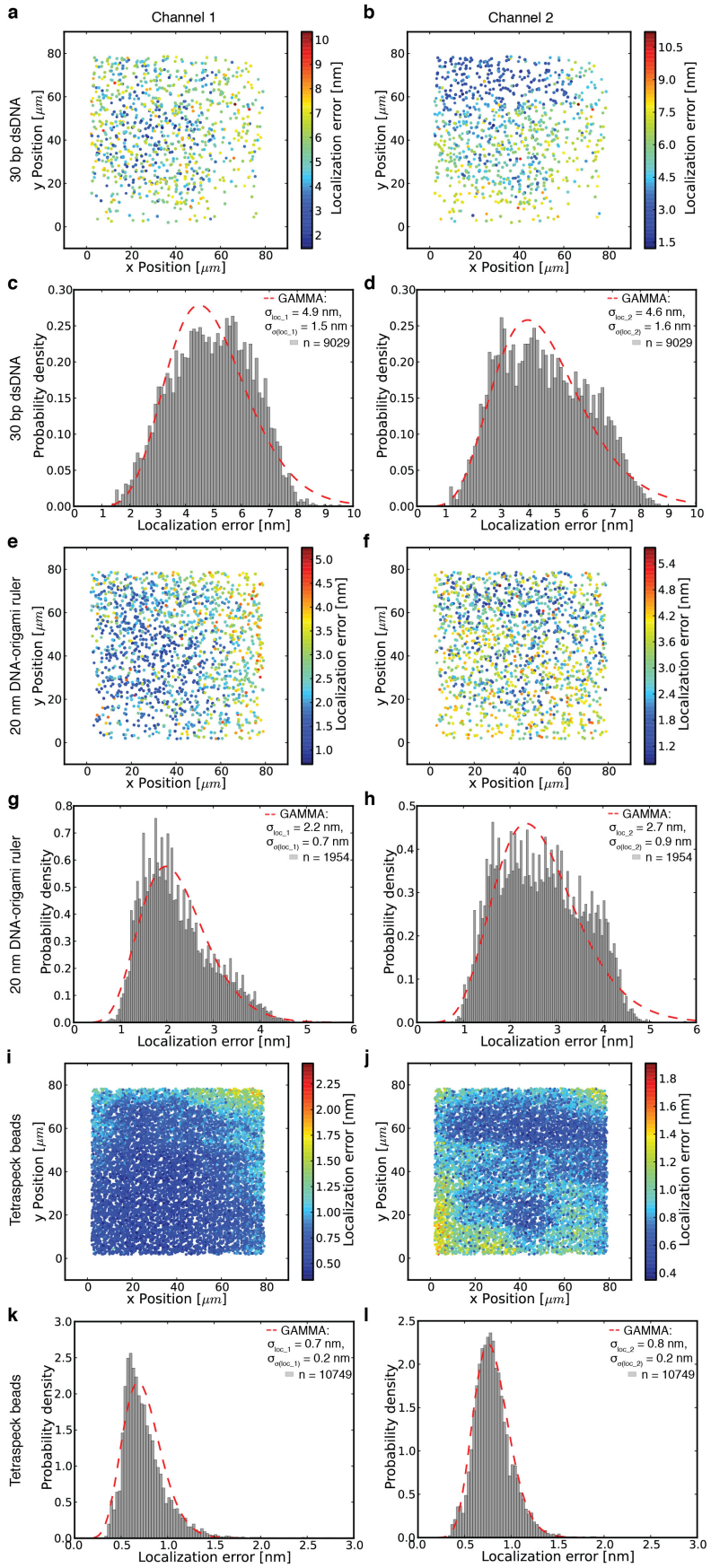
a
Channel 1
b
Channel 2
30 bp dsDNA
y Position [μm]
x Position [μm]
Localization error [nm]
c
d
Probability density
GAMMA:
σ_loc_1 = 4.9 nm,
σ_σ(loc_1) = 1.5 nm
n = 9029
σ_loc_2 = 4.6 nm,
σ_σ(loc_2) = 1.6 nm
n = 9029
Localization error [nm]
e
f
20 nm DNA-origami ruler
g
h
σ_loc_1 = 2.2 nm,
σ_σ(loc_1) = 0.7 nm
n = 1954
σ_loc_2 = 2.7 nm,
σ_σ(loc_2) = 0.9 nm
n = 1954
i
j
Tetraspeck beads
k
l
σ_loc_1 = 0.7 nm,
σ_σ(loc_1) = 0.2 nm
n = 10749
σ_loc_2 = 0.8 nm,
σ_σ(loc_2) = 0.2 nm
n = 10749

Supplementary Figure 5 | Localization errors over entire field of view for three different probes in two channels. Quantification of 30 bp dsDNA constructs with a Cy3 dye on one and a Cy5 dye on the other end (**a-d**), of 20 nm DNA-origami nanorulers with 5-10 dyes of Cy3 and 5-10 dyes of Alexa 647 whose center of mass is 20 nm apart (**e-h**), and of TetraSpeck beads (**i-l**). (**a**) Localization errors calculated with MLEwG equation from Mortensen et al.[3] in channel 1 (Cy3 or Cy3 like dye(s)) for 30 bp dsDNA construct. Red dots indicate high and blue dots low localization errors. (**b**) Same as in **a** but for channel 2 (Cy5 or Cy5 like dye(s)). (**c**) Histogram of localization error in channel 1 for 30 bp dsDNA construct with fit of gamma distribution (dashed red line) of data shown in **a**. (**d**) Same as in **c** but for channel 2. (**e-h**) Same as in **a**-**d** but for 20 nm DNA-origami nanoruler. (**i-l**) Same as in **a**-**d** but for TetraSpeck beads. For 30 bp dsDNA construct and for 20 nm DNA-origami nanoruler 20 frames per molecule were recorded. For TetraSpeck beads one frame per molecules was acquired. Details about fitting parameters in **Supplementary Table 3**.

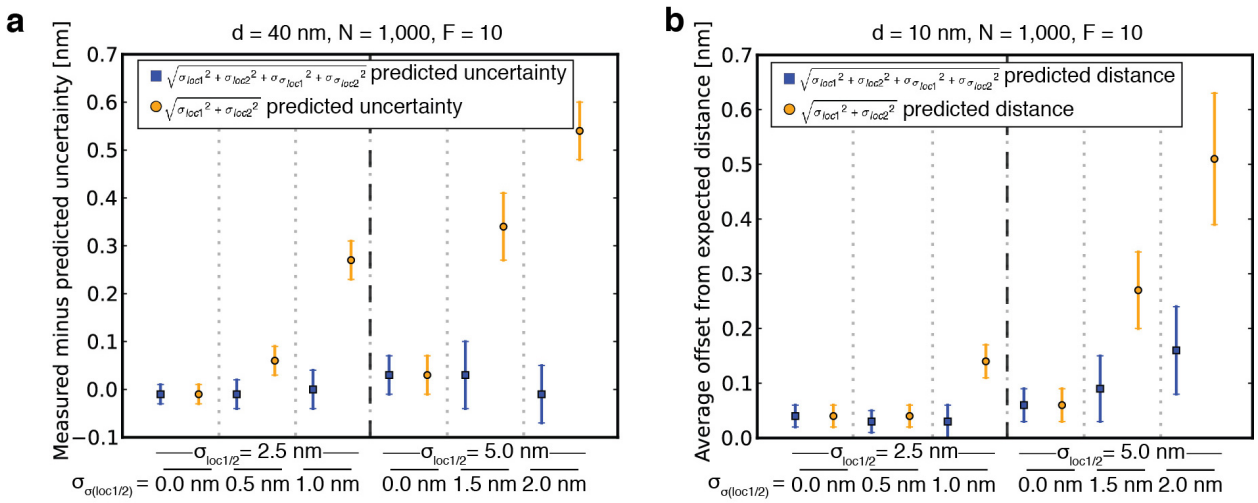

Supplementary Figure 6 | Influence of standard deviation of localization errors on accurate distance prediction. (**a**) 10 repeats of Monte Carlo simulated data with a 40 nm true distance (d), 10 frames (F), and 1,000 pairs (N). The distance uncertainty σ_d was varied by changing localization errors (σ_{loc_1}, σ_{loc_2}) and standard deviation of the localization errors ($\sigma_{\sigma(loc_1)}$, $\sigma_{\sigma(loc_2)}$). Similar to NeNA[4] we used Churchman-P2D to calculate the measured distance uncertainty and subtracted the predicted uncertainty based on either only the localization errors (orange) or localization errors and their underlying standard deviation (blue). Note: We used a true distance of 40 nm because that allows us to apply Churchman-P2D since $d > \sigma_d$. (**b**) 10 repeats of Monte Carlo simulated data with a 10 nm true distance (d), 10 frames (F), and 1,000 pairs (N). The distance uncertainty was varied by changing localization errors (σ_{loc_1}, σ_{loc_2}) and standard deviation of the localization errors ($\sigma_{\sigma(loc_1)}$, $\sigma_{\sigma(loc_2)}$). The measured distance μ was determined by means of Avg-Sigma-P2D using either only the localization errors (orange) or localization errors and their underlying standard deviation (blue). Subsequently the average offset from the expected distance was calculated for both cases. Error bars show standard deviation of 10 independent simulations.

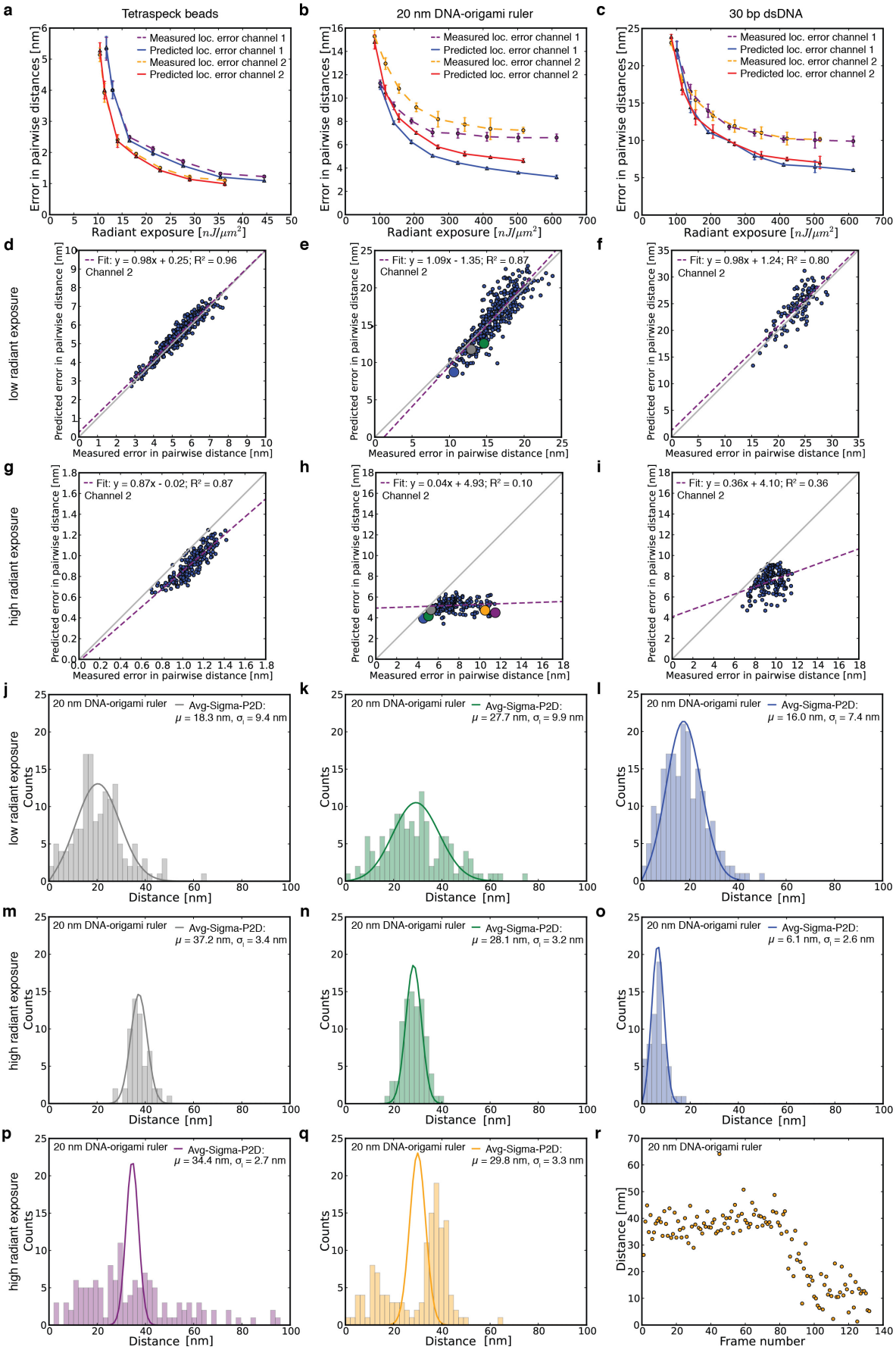
a
Tetraspeck beads
b
20 nm DNA-origami ruler
c
30 bp dsDNA
Measured loc. error channel 1
Predicted loc. error channel 1
Measured loc. error channel 2
Predicted loc. error channel 2
Error in pairwise distances [nm]
Radiant exposure [$nJ/\mu m^2$]
d
e
f
g
h
i
low radiant exposure
high radiant exposure
Fit: y = 0.98x + 0.25; R² = 0.96
Channel 2
Fit: y = 1.09x - 1.35; R² = 0.87
Channel 2
Fit: y = 0.98x + 1.24; R² = 0.80
Channel 2
Fit: y = 0.87x - 0.02; R² = 0.87
Channel 2
Fit: y = 0.04x + 4.93; R² = 0.10
Channel 2
Fit: y = 0.36x + 4.10; R² = 0.36
Channel 2
Predicted error in pairwise distance [nm]
Measured error in pairwise distance [nm]
j
k
l
m
n
o
p
q
r
20 nm DNA-origami ruler
Avg-Sigma-P2D:
μ = 18.3 nm, σ_l = 9.4 nm
μ = 27.7 nm, σ_l = 9.9 nm
μ = 16.0 nm, σ_l = 7.4 nm
μ = 37.2 nm, σ_l = 3.4 nm
μ = 28.1 nm, σ_l = 3.2 nm
μ = 6.1 nm, σ_l = 2.6 nm
μ = 34.4 nm, σ_l = 2.7 nm
μ = 29.8 nm, σ_l = 3.3 nm
Counts
Distance [nm]
Frame number

Supplementary Figure 7 | Comparison of measured and predicted localization errors for three different probes in two channels. Quantification of TetraSpeck beads (**a, d, g**), of 20 nm DNA-origami nanorulers with 5-10 dyes of Cy3 and 5-10 dyes of Alexa 647 whose center of mass is 20 nm apart (**b, e, h**), and of 30 bp dsDNA constructs with a Cy3 dye on one and a Cy5 dye on the other end (**c, f, i**). (**a-c**) Predicted errors in pairwise distances calculated with MLEwG equation from Mortensen et al.[3] for channel 1 (Cy3 or Cy3 like dye(s)) in blue and channel 2 (Cy5 or Cy5 like dye(s)) in red as function of radiant exposure (**Supplementary Table 2**). Measured error (standard deviation) in pairwise distances for channel 1 in purple and channel 2 in orange as function of radiant exposure. (**d-f**) Scatter plot of predicted over measure error in pairwise distances of individual molecules (blue dots) for lowest radiant exposure in channel 2 from data in **a**-**c**. Dashed purple line shows fit of linear regression and gray solid line shows theoretical limit (Cramér–Rao lower bound[5]) for localization errors. (**g-i**) Same as in **d**-**f** but for highest radiant exposure setting. (**e**) Larger, colored dots refer to histograms shown in **j**-**l**. (**h**) Larger, colored dots refer to histograms shown in **m**-**q**. (**j-l**) Histogram of distance distribution of a single-molecule of a 20 nm DNA-origami nanoruler at low radiant exposure. Solid line is fit with Avg-Sigma-P2D. (**m-q**) Same as **j**-**l** but at high radiant exposure. (**r**) Distance as a function of time (frame number) of a single-molecule of a 20 nm DNA-origami nanoruler (orange dots). Same data as shown in **q**. Error bars in **a**-**c** show standard deviation of three repeats (new microscopy slides with fresh sample). Each repeat consists of at least 120 pairwise distance measurements and the minimum for number of frames per molecule was set to 60 and the maximum number of frames is 200. Single-molecule distances in **j-r** were obtained by selecting time-lapse series of individual molecules (see **Supplementary Table 5**). Details about fitting parameters in **Supplementary Table 3**.

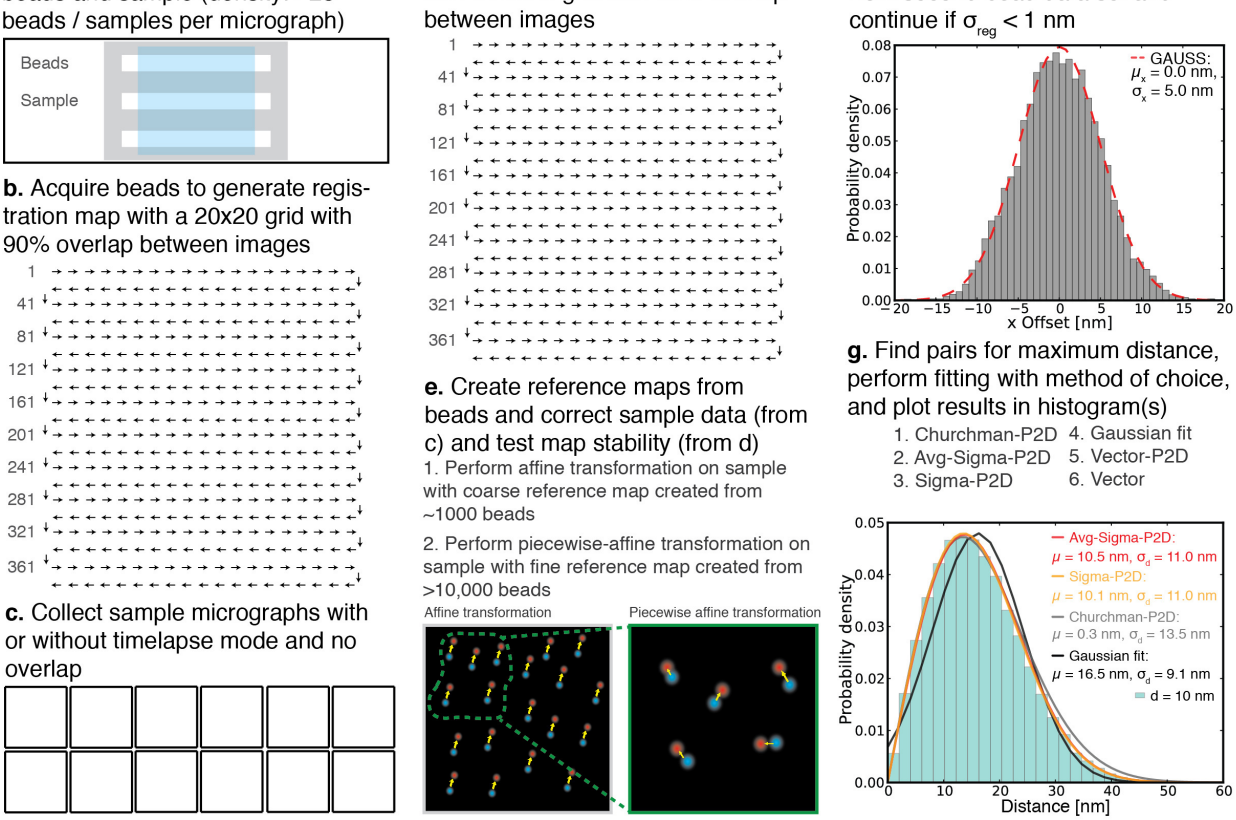

Supplementary Figure 8 | Workflow for image registration and distance measurements. (**a**) Set-up of microscope slide with fiducial markers in one and sample of interest in another chamber. (**b**) Image acquisition pattern for fiducial markers to create registration map. (**c**) Image acquisition pattern for sample of interest. (**d**) Same as in **b** but this time to test the registration map after sample data collection. (**e**) μManager[1] analysis procedure to create affine and piecewise affine registration maps. (**f**) Calculation of image registration accuracy. (**g**) μManager[1] analysis procedure to determine distance distribution with various methods. For more details see **Supplementary Protocol**.

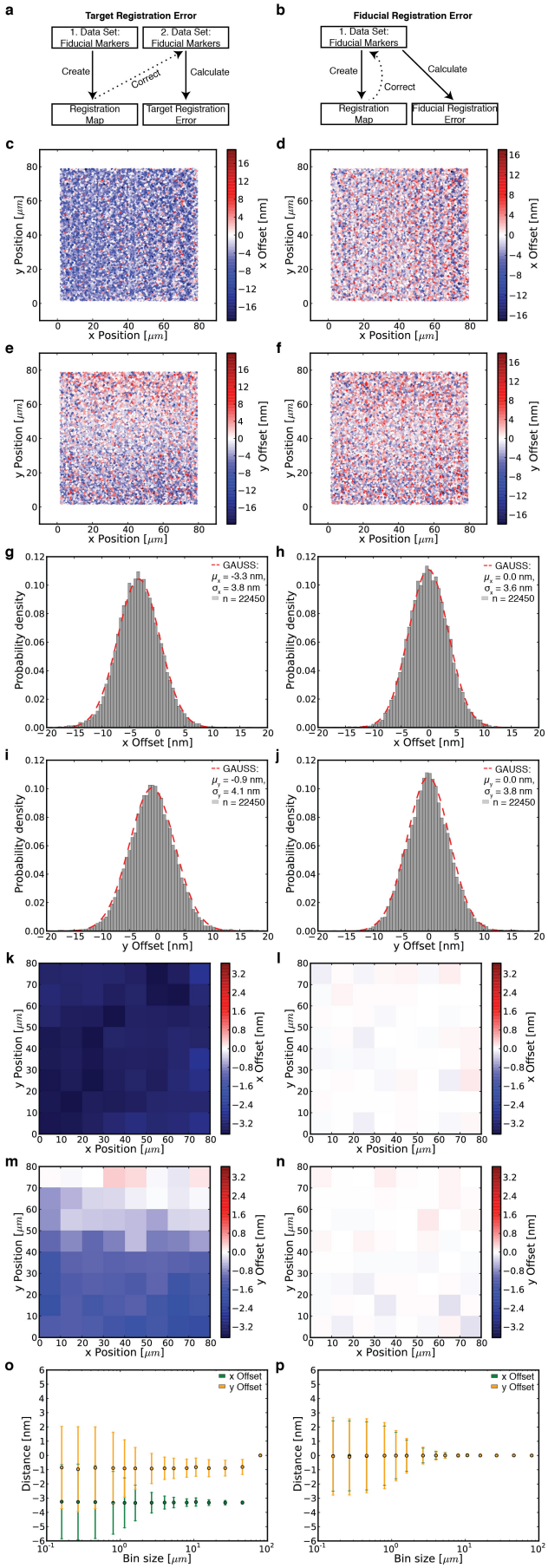
a
Target Registration Error
1. Data Set: Fiducial Markers
2. Data Set: Fiducial Markers
Create
Correct
Calculate
Registration Map
Target Registration Error
b
Fiducial Registration Error
1. Data Set: Fiducial Markers
Create
Correct
Calculate
Registration Map
Fiducial Registration Error
c
d
e
f
y Position [μm]
x Position [μm]
x Offset [nm]
y Offset [nm]
g
h
i
j
GAUSS:
μ_x = -3.3 nm,
σ_x = 3.8 nm
n = 22450
μ_x = 0.0 nm,
σ_x = 3.6 nm
n = 22450
μ_y = -0.9 nm,
σ_y = 4.1 nm
n = 22450
μ_y = 0.0 nm,
σ_y = 3.8 nm
n = 22450
Probability density
x Offset [nm]
y Offset [nm]
k
l
m
n
o
p
x Offset
y Offset
Distance [nm]
Bin size [μm]

Supplementary Figure 9 | Comparison of target registration error (TRE) and fiducial registration error (FRE). Note that FRE and TRE are uncorrelated[6] and misleading cases - as shown here - can be observed where the FRE is zero but the TRE is large. (**a**) Workflow for how target registration error (TRE) is calculated. (**b**) Workflow for how fiducial registration error (FRE) is calculated. (**c-p**) Same map is used for both, TRE and FRE, but different data sets are used to test the map. (**c**) Distance offset along the x-axis for TRE. Negative values (blue dots) mean that channel 1 has a smaller number for its x position whereas positive values (red dots) represent fiducials where channel 2 has a smaller number for its x position. (**d**) Same as in **c** but for FRE. (**e**) Distance offset along the y-axis for TRE. Negative values (blue dots) mean that channel 1 has a smaller number for its y position whereas positive values (red dots) represent fiducials where channel 2 has a smaller number for its y position. (**f**) Same as in **e** but for FRE. (**g**) Histogram of x-axis offset with Gaussian fit (dashed red line) for TRE. (**h**) Same as in **g** but for FRE. (**i**) Histogram of y-axis offset with Gaussian fit (dashed red line) for TRE. (**j**) Same as in **i** but for FRE. (**k**) Same as in **c** but with a binning of 10 µm by 10 µm boxes. (**l**) Same as in **d** but with a binning of 10 µm by 10 µm boxes. (**m**) Same as in **e** but with a binning of 10 µm by 10 µm boxes. (**n**) Same as in **f** but with a binning of 10 µm by 10 µm boxes. (**o**) Average offset along x-axis (green) and y-axis (orange) as a function of bin size for TRE. Markers indicate average offset of all boxes created with respective bin size. Error bars show standard deviation from average offset of all boxes created with respective bin size. (**p**) Same as in **o** but for FRE. One frame per TetraSpeck bead was acquired. Details about fitting parameters in **Supplementary Table 3**.

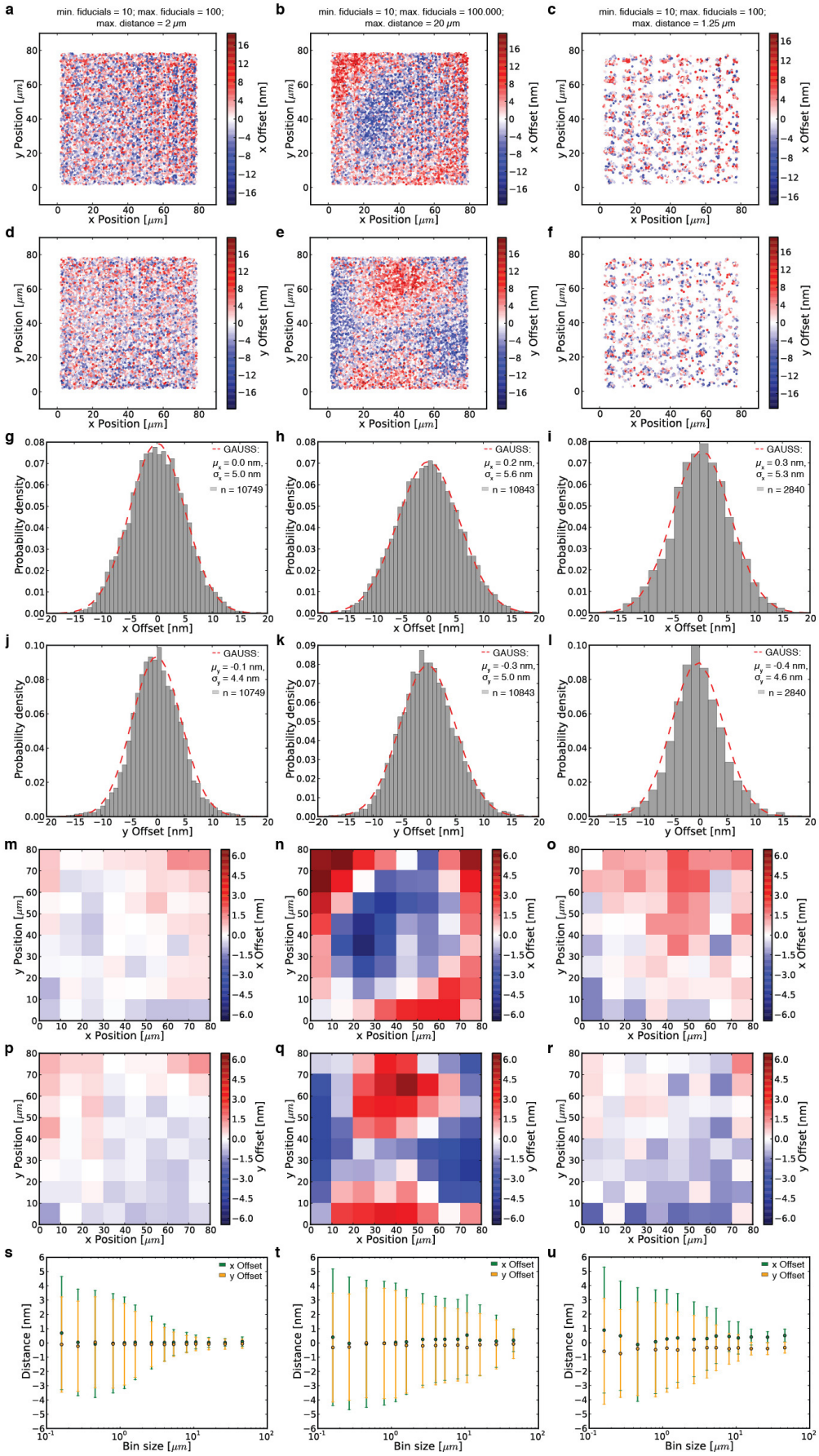
a
min. fiducials = 10; max. fiducials = 100;
max. distance = 2 μm
b
min. fiducials = 10; max. fiducials = 100.000;
max. distance = 20 μm
c
min. fiducials = 10; max. fiducials = 100;
max. distance = 1.25 μm
x Position [μm]
y Position [μm]
x Offset [nm]
d
e
f
y Offset [nm]
g
GAUSS:
μx = 0.0 nm,
σx = 5.0 nm
n = 10749
h
GAUSS:
μx = 0.2 nm,
σx = 5.6 nm
n = 10843
i
GAUSS:
μx = 0.3 nm,
σx = 5.3 nm
n = 2840
Probability density
x Offset [nm]
j
GAUSS:
μy = -0.1 nm,
σy = 4.4 nm
n = 10749
k
GAUSS:
μy = -0.3 nm,
σy = 5.0 nm
n = 10843
l
GAUSS:
μy = -0.4 nm,
σy = 4.6 nm
n = 2840
y Offset [nm]
m
n
o
p
q
r
s
x Offset
y Offset
t
u
Distance [nm]
Bin size [μm]

Supplementary Figure 10 | Comparison of different parameters for piecewise affine image registration. The first parameter setting has a minimum of 10 and maximum of 100 fiducial points as well as a maximum distance of 2 μm. The second parameter setting has a minimum of 10 and maximum of 100,000 fiducial points as well as a maximum distance of 20 μm. And the third parameter setting has a minimum of 10 and maximum of 100 fiducial points as well as a maximum distance of 1.25 μm. (**a**) Distance offset along the x-axis for first setting. Negative values (blue dots) mean that channel 1 has a smaller number for its x position whereas positive values (red dots) represent fiducials where channel 2 has a smaller number for its x position. (**b**) Same as in **a** but for second setting. (**c**) Same as in **a** but for third setting. (**d**) Distance offset along the y-axis for first setting. Negative values (blue dots) mean that channel 1 has a smaller number for its y position whereas positive values (red dots) represent fiducials where channel 2 has a smaller number for its y position. (**e**) Same as in **d** but for second setting. (**f**) Same as in **d** but for third setting. (**g**) Histogram of x-axis offset with Gaussian fit (dashed red line) of data in **a**. (**h**) Same as in **g** but for second setting and of data in **b**. (**i**) Same as in **g** but for third setting and of data in **c**. (**j**) Histogram of y-axis offset with Gaussian fit (dashed red line) of data in **d**. (**k**) Same as in **j** but for second setting and of data in **e**. (**l**) Same as in **j** but for third setting and of data in **f**. (**m**) Same as in **a** but with a binning of 10 μm by 10 μm boxes. (**n**) Same as in **b** but with a binning of 10 μm by 10 μm boxes. (**o**) Same as in **c** but with a binning of 10 μm by 10 μm boxes. (**p**) Same as in **d** but with a binning of 10 μm by 10 μm boxes. (**q**) Same as in **e** but with a binning of 10 μm by 10 μm boxes. (**r**) Same as in **f** but with a binning of 10 μm by 10 μm boxes. (**s**) Average offset along x-axis (green) and y-axis (orange) as a function of bin size for first parameter setting. Markers indicate average offset of all boxes created with respective bin size. Error bars show standard deviation from average offset of all boxes created with respective bin size. (**t**) Same as in **s** but for second setting. (**u**) Same as in **s** but for third setting. Details about fitting parameters in **Supplementary Table 3**.

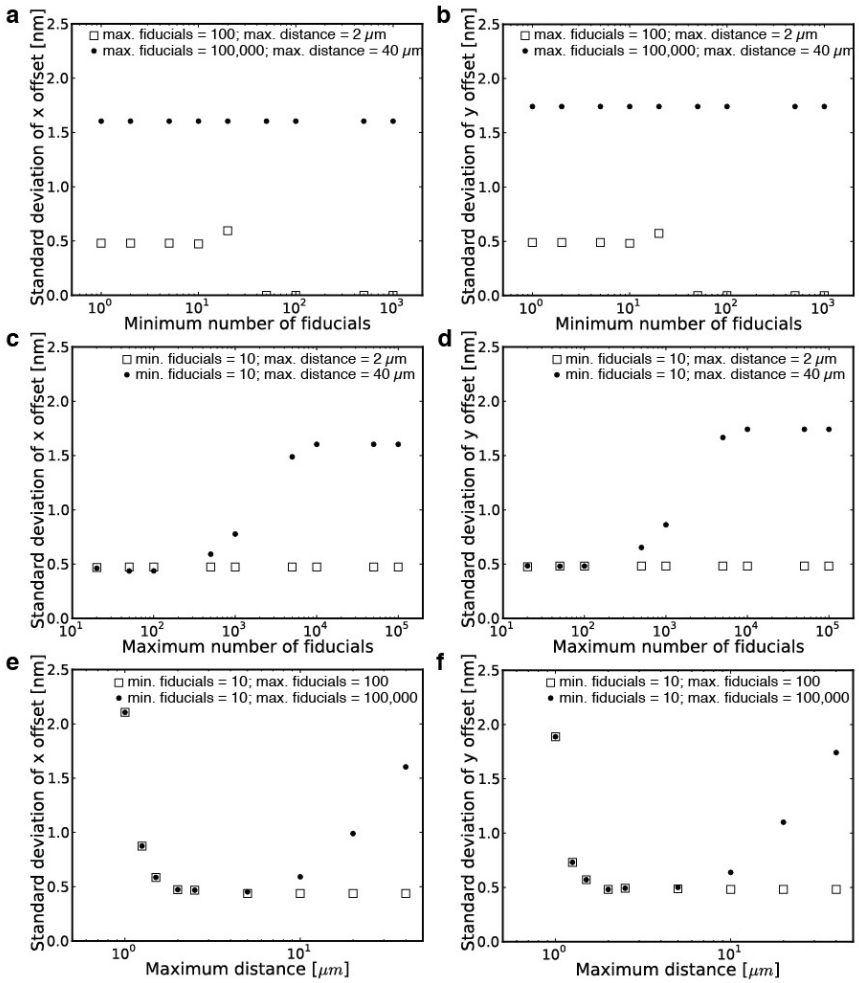

Supplementary Figure 11 | In-depth quantification of different parameters for pairwise affine image registration. Bin size for all calculations is 10 μm by 10 μm. (**a**) Standard deviation from average offset along x-axis of all boxes as a function of minimum number of fiducials. Results are shown for two different settings of maximum number of fiducials and maximum distance (filled circle and empty square). (**b**) Same as in **a** but along y-axis. (**c**) Standard deviation from average offset along x-axis of all boxes as a function of maximum number of fiducials. Results are shown for two different settings of minimum number of fiducials and maximum distance (filled circle and empty square). (**d**) Same as in **c** but along y-axis. (**e**) Standard deviation from average offset along x-axis of all boxes as a function of maximum distance. Results are shown for two different settings of minimum and maximum number of fiducials (filled circle and empty square). (**f**) Same as in **e** but along y-axis. Details about fitting parameters in **Supplementary Table 3**.

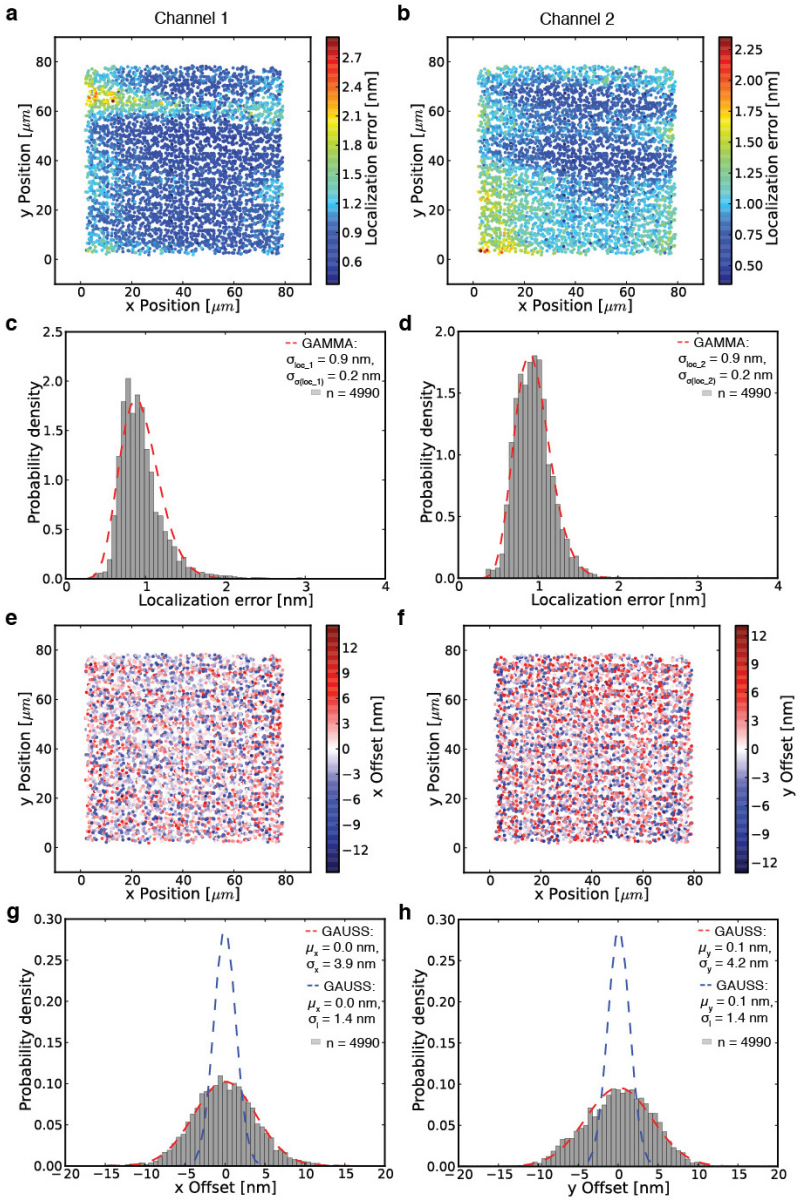

Supplementary Figure 12 | Registration precision of TetraSpeck beads can not solely be explained by localization errors. (**a**) Localization errors in channel 1 of TetraSpeck beads over the entire field of view calculated with MLEwG equation from Mortensen et al.[3]. Red dots indicate high and blue dots low localization errors. (**b**) Same as in **a** but for channel 2. (**c**) Histogram of localization errors in channel 1 with fit of gamma distribution (dashed red line) of data shown in **a**. (**d**) Same as in **c** but for channel 2 and of data in **b**. (**e**) Distance offset along the x-axis for same data as shown in **a**. Negative values (blue dots) mean that channel 1 has a smaller number for its x position whereas positive values (red dots) represent fiducials where channel 2 has a smaller number for its x position. (**f**) Same as in **e** but for distance offset along

y-axis. (**g**) Histogram of x-axis offset with Gaussian fit (dashed red line) of data in **e**. Blue dashed line shows fit if σ_x was only comprised of the localization error σ_l. (**h**) Same as in **g** but for offset along y-axis and of data in **f**. One frame per TetraSpeck bead was acquired. Details about fitting parameters in **Supplementary Table 3**.

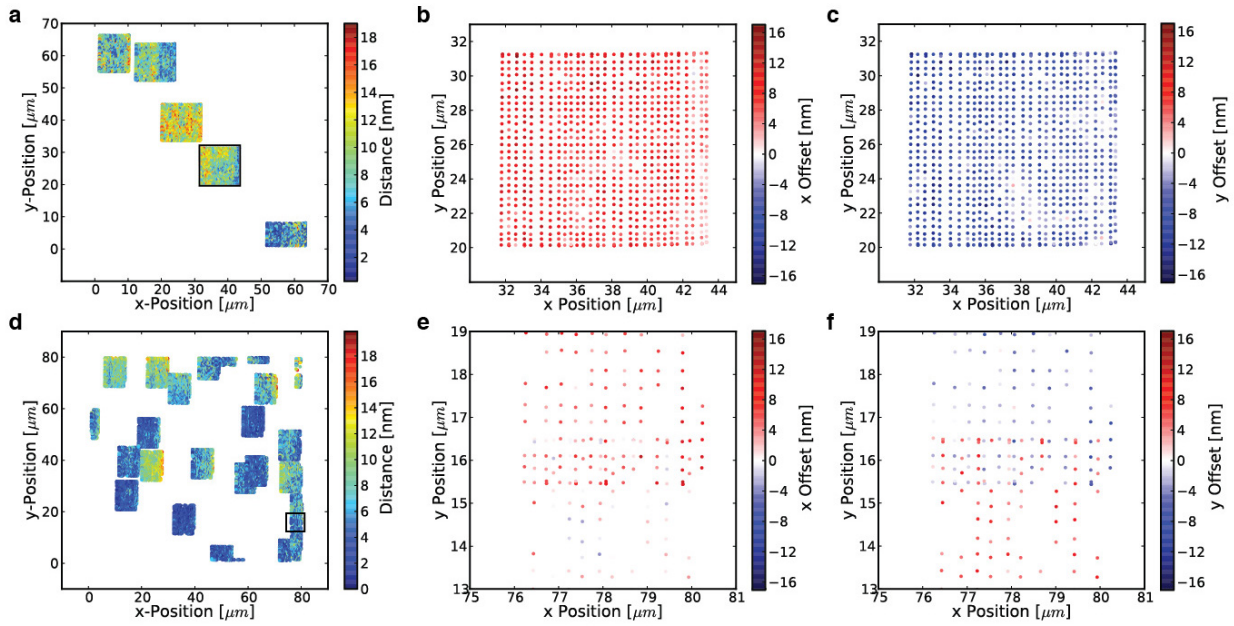

Supplementary Figure 13 | TetraSpeck beads have an underlying heterogeneity and not a true distance of zero nanometer. (**a**) Euclidean distance of image registered, 30x30 grid translated, TetraSpeck beads. Each grid shows data for one and the same bead. Red dots indicate large and blue dots short distances. Black box highlights area which is shown with higher magnification in **b** and **c**. (**b**) Distance offset along the x-axis of magnified part of micrograph in **a**. (**c**) Same as in **b** but distance offset along y-axis. (**d**) Euclidean distance of image registered, 20x30 grid translated TetraSpeck beads. Each grid shows data for one and the same bead. Red dots indicate large and blue dots short distances. Black box highlights area which is shown with higher magnification in **e** and **f**. (**e**) Distance offset along the x-axis of magnified part of micrograph in **d**. (**f**) Same as in **e** but distance offset along y-axis. Details about fitting parameters in **Supplementary Table 3**.

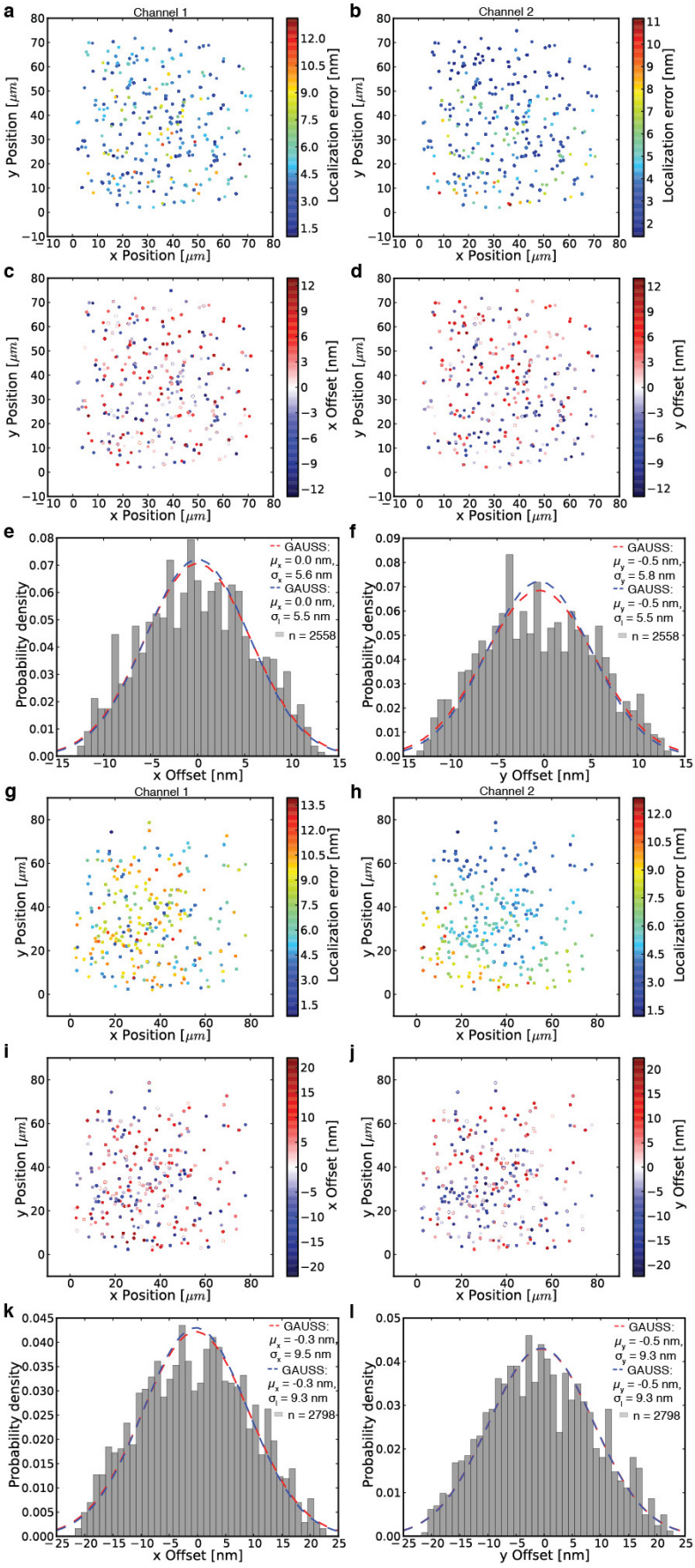
a
Channel 1
b
Channel 2
y Position [μm]
x Position [μm]
Localization error [nm]
c
d
x Offset [nm]
y Offset [nm]
e
f
Probability density
GAUSS:
μ_x = 0.0 nm,
σ_x = 5.6 nm
GAUSS:
μ_x = 0.0 nm,
σ_l = 5.5 nm
n = 2558
μ_y = -0.5 nm,
σ_y = 5.8 nm
μ_y = -0.5 nm,
σ_l = 5.5 nm
g
h
i
j
k
μ_x = -0.3 nm,
σ_x = 9.5 nm
μ_x = -0.3 nm,
σ_l = 9.3 nm
n = 2798
l
μ_y = -0.5 nm,
σ_y = 9.3 nm
μ_y = -0.5 nm,
σ_l = 9.3 nm

Supplementary Figure 14 | Registration precision can solely be explained by the localization errors σ_l for a single biotinylated Cy3/Cy5 dsDNA construct. (**a**) Localization errors in channel 1 of Cy3/Cy5 dsDNA construct over the entire field of view calculated with MLEwG equation from Mortensen et al.[3]. Red dots indicate high and blue dots low localization errors. (**b**) Same as in **a** but for channel 2. (**c**) Distance offset along the x-axis for same data as shown in **a**. Negative values (blue dots) mean that channel 1 has a smaller number for its x position whereas positive values (red dots) represent fiducials where channel 2 has a smaller number for its x position. (**d**) Same as in **c** but for distance offset along y-axis. (**e**) Histogram of x-axis offset with Gaussian fit (dashed red line) of data in **c**. Blue dashed line shows fit if σ_x was only comprised of the localization error σ_l. (**f**) Same as in **e** but for offset along y-axis and of data in **d**. (**g-l**) Same as **a**-**f** but at lower radiant exposure. 20 frames of each molecule were collected. Details about fitting parameters in **Supplementary Table 3**.

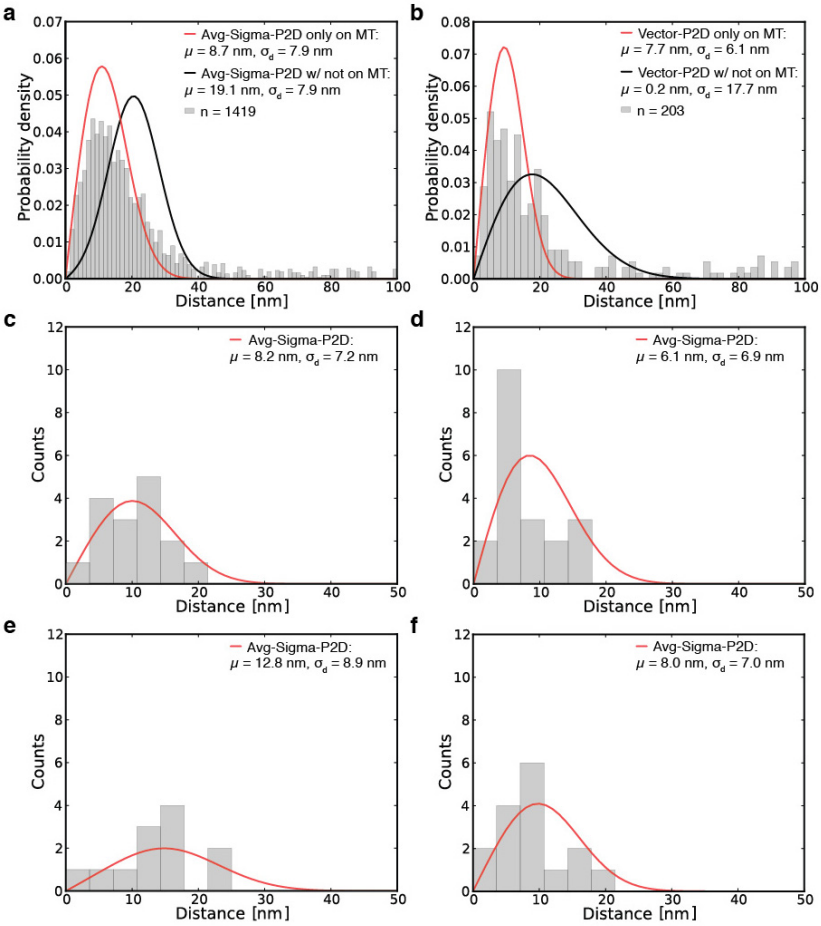

Supplementary Figure 15 | Influence of background on head-to-head distance of a rigor-bound kinesin. (**a**) Histogram of head-to-head distance measurements of rigor-bound kinesin with background (not microtubule bound kinesin) fitted with Avg-Sigma-P2D (black) and if background is not taken into account as in Figure 4 (red). (**b**) Histogram of vector averaged head-to-head distance measurements of rigor-bound kinesin with background (not microtubule bound kinesin) fitted with Vector-P2D (black) and if background is not taken into account as in Figure 4 (red). (**c-f**) Histogram of a single-molecule of head-to-head distance measurements of rigor-bound kinesin fitted with Avg-Sigma-P2D (red). Single-molecule distances in **a-f** were obtained by selecting time-lapse series of individual molecules (see **Supplementary Table 5**). Details about fitting parameters in **Supplementary Table 3**.

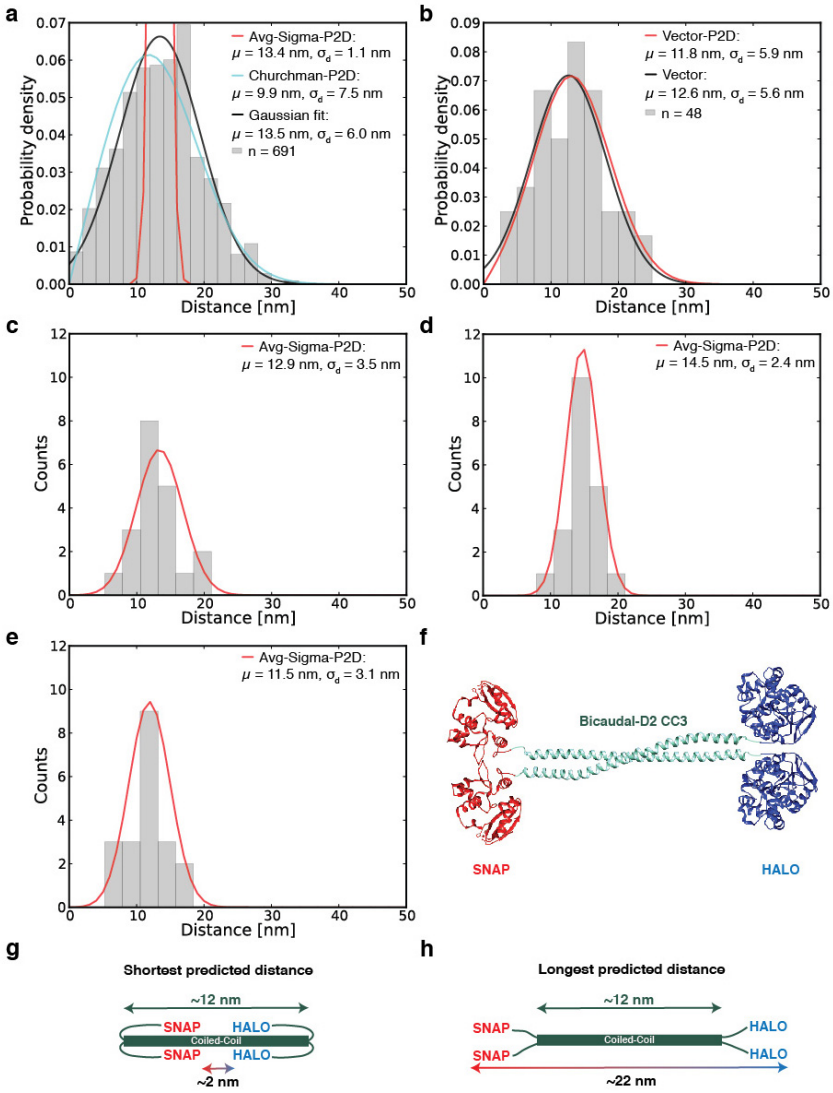

Supplementary Figure 16 | Conformational heterogeneity of end-to-end distance of Bicaudal D2 CC3. (**a**) Histogram of end-to-end distance measurements of Bicaudal D2 CC3 using a higher threshold for noise tolerance as in **Figure 5** fitted with Avg-Sigma-P2D (red), Churchman-P2D (cyan), and Gaussian fit (black). (**b**) Histogram of vector averaged end-to-end distance measurements of Bicaudal D2 CC3 using a higher threshold for noise tolerance as in **Figure 5** analyzed with Vector-P2D (red) and Vector (black). (**c-e**) Histogram of distance measurements of a single-molecule of Bicaudal D2 CC3 fitted with Avg-Sigma-P2D (red). (**f**) Detailed diagram of SNAP[7] and HALO[8] labeled Bicaudal D2 CC3 based on crystal structures (PDB: 4BL6[9], 3L00[10], 5UXZ[11]) and created with UCSF Chimera[12]. (**g-h**) Schematic of conformations of SNAP[7] and HALO[8] labeled Bicaudal D2 CC3 that lead to possible shortest (**g**) and longest (**h**) distance. Single-molecule distances in **a-e** were obtained by selecting

time-lapse series of individual molecules (see **Supplementary Table 5**). Details about fitting parameters in **Supplementary Table 3**.

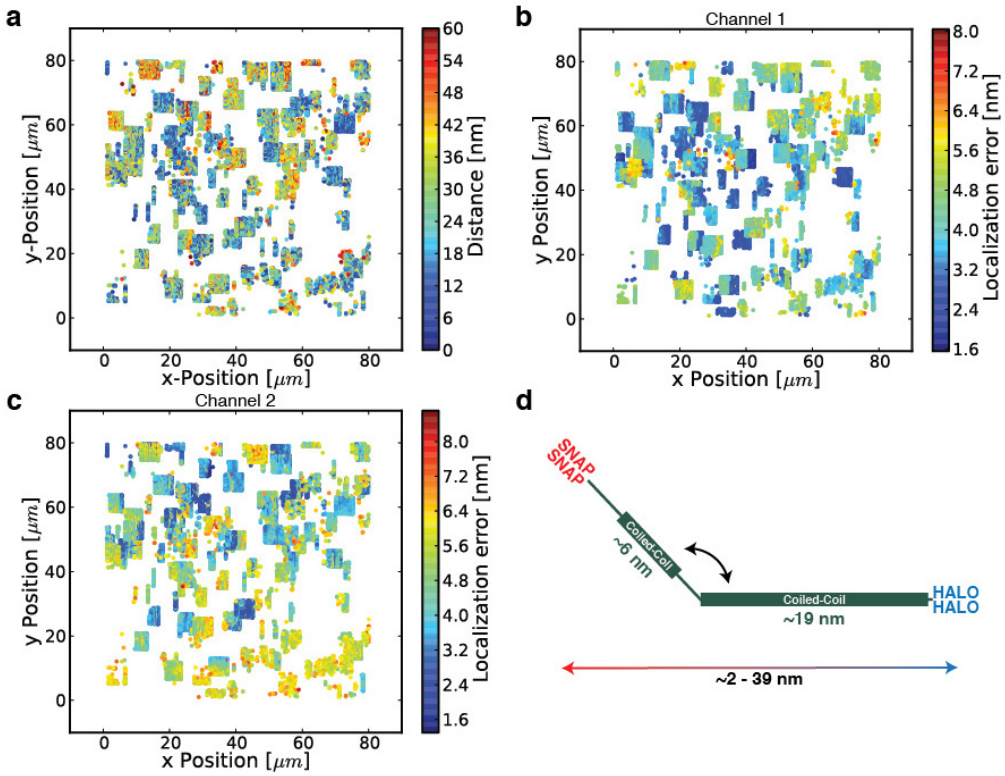

Supplementary Figure 17 | Conformational heterogeneity of end-to-end distance of Bicaudal D2 CC1. (**a**) Euclidean distance of image registered, 16x16 grid translated, Bicaudal D2 CC1. Each grid shows data for one and the same molecule. Red dots indicate large and blue dots short distances. (**b**) Localization errors in channel 1 of Bicaudal D2 CC1 over the entire field of view calculated with MLEwG equation from Mortensen et al.[3]. Red dots indicate high and blue dots low localization errors. (**c**) Same as in **b** but for channel 2. (**d**) Schematic of possible conformations of SNAP[7] and HALO[8] labeled Bicaudal D2 CC1 that lead to a broad distance distribution. Details about fitting parameters in **Supplementary Table 3**.

```
Mus BICD2      20  EWLRAEVKRLSHELAETTREKIQAAEYGLAVLEEKHQLKLQFEELEVDYEAIRSEMEQLKEAFGQAHTNHKKVAADGESREESLIQESAS    110
SS_PSIPRED         HHHH
```

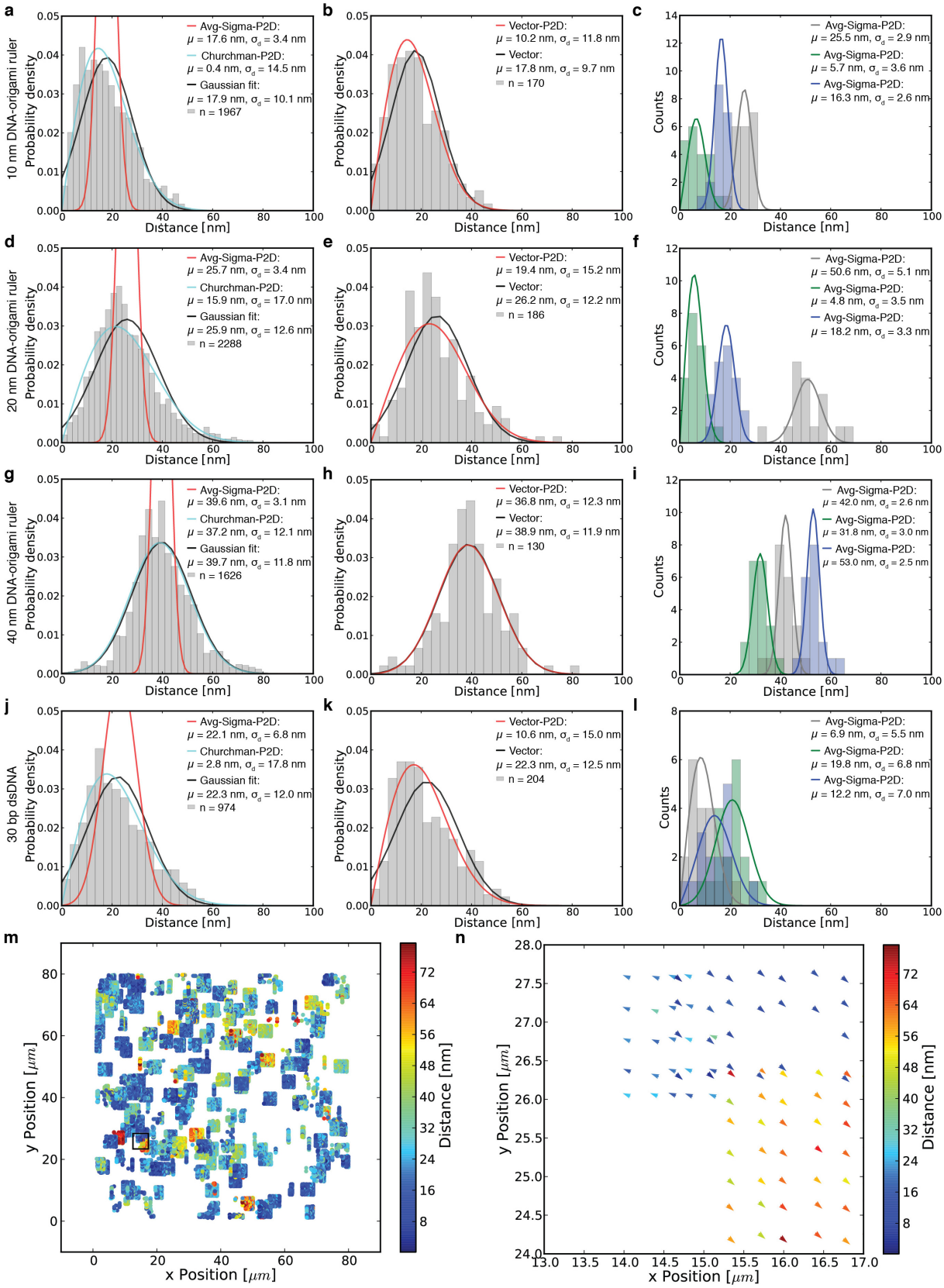
a
10 nm DNA-origami ruler
Probability density
Avg-Sigma-P2D:
μ = 17.6 nm, σd = 3.4 nm
Churchman-P2D:
μ = 0.4 nm, σd = 14.5 nm
Gaussian fit:
μ = 17.9 nm, σd = 10.1 nm
n = 1967
Distance [nm]
b
Probability density
Vector-P2D:
μ = 10.2 nm, σd = 11.8 nm
Vector:
μ = 17.8 nm, σd = 9.7 nm
n = 170
Distance [nm]
c
Counts
Avg-Sigma-P2D:
μ = 25.5 nm, σd = 2.9 nm
Avg-Sigma-P2D:
μ = 5.7 nm, σd = 3.6 nm
Avg-Sigma-P2D:
μ = 16.3 nm, σd = 2.6 nm
Distance [nm]
d
20 nm DNA-origami ruler
Probability density
Avg-Sigma-P2D:
μ = 25.7 nm, σd = 3.4 nm
Churchman-P2D:
μ = 15.9 nm, σd = 17.0 nm
Gaussian fit:
μ = 25.9 nm, σd = 12.6 nm
n = 2288
Distance [nm]
e
Probability density
Vector-P2D:
μ = 19.4 nm, σd = 15.2 nm
Vector:
μ = 26.2 nm, σd = 12.2 nm
n = 186
Distance [nm]
f
Counts
Avg-Sigma-P2D:
μ = 50.6 nm, σd = 5.1 nm
Avg-Sigma-P2D:
μ = 4.8 nm, σd = 3.5 nm
Avg-Sigma-P2D:
μ = 18.2 nm, σd = 3.3 nm
Distance [nm]
g
40 nm DNA-origami ruler
Probability density
Avg-Sigma-P2D:
μ = 39.6 nm, σd = 3.1 nm
Churchman-P2D:
μ = 37.2 nm, σd = 12.1 nm
Gaussian fit:
μ = 39.7 nm, σd = 11.8 nm
n = 1626
Distance [nm]
h
Probability density
Vector-P2D:
μ = 36.8 nm, σd = 12.3 nm
Vector:
μ = 38.9 nm, σd = 11.9 nm
n = 130
Distance [nm]
i
Counts
Avg-Sigma-P2D:
μ = 42.0 nm, σd = 2.6 nm
Avg-Sigma-P2D:
μ = 31.8 nm, σd = 3.0 nm
Avg-Sigma-P2D:
μ = 53.0 nm, σd = 2.5 nm
Distance [nm]
j
30 bp dsDNA
Probability density
Avg-Sigma-P2D:
μ = 22.1 nm, σd = 6.8 nm
Churchman-P2D:
μ = 2.8 nm, σd = 17.8 nm
Gaussian fit:
μ = 22.3 nm, σd = 12.0 nm
n = 974
Distance [nm]
k
Probability density
Vector-P2D:
μ = 10.6 nm, σd = 15.0 nm
Vector:
μ = 22.3 nm, σd = 12.5 nm
n = 204
Distance [nm]
l
Counts
Avg-Sigma-P2D:
μ = 6.9 nm, σd = 5.5 nm
Avg-Sigma-P2D:
μ = 19.8 nm, σd = 6.8 nm
Avg-Sigma-P2D:
μ = 12.2 nm, σd = 7.0 nm
Distance [nm]
m
y Position [μm]
x Position [μm]
Distance [nm]
n
y Position [μm]
x Position [μm]
Distance [nm]

Supplementary Figure 19 | Distance measurements for DNA-origami nanorulers and 30 bp dsDNA construct. (**a**) Histogram of distance measurements of 10 nm DNA-origami nanoruler fitted with Avg-Sigma-P2D (red), Churchman-P2D (cyan), and Gaussian fit (black). (**b**) Histogram of vector averaged distance measurements of 10 nm DNA-origami nanoruler analyzed with Vector-P2D (red) and Vector (black). (**c**) Histogram of distance distribution of three different single-molecule 10 nm DNA-origami nanorulers (green, blue, and gray). Solid line is fit with Avg-Sigma-P2D. (**d-f**) Same as **a**-**c** but for 20 nm DNA-origami nanoruler. (**g-i**) Same as **a**-**c** but for 30 nm DNA-origami nanoruler. (**j-l**) Same as **a**-**c** but for 30bp (≅10 nm) dual biotinylated Cy3/Cy5 dsDNA construct. (**m**) Euclidean distance of image registered, 12x12 grid translated, 20 nm DNA-origami nanoruler. Each grid shows data for one and the same ruler. Red dots indicate large and blue dots short distances. Black box highlights area which is shown with higher magnification in **n**. (**n**) Magnification of highlighted part of micrograph in **a**. Arrowheads point from position of molecule in channel 1 to its position in channel 2. Red arrowheads indicate large and blue arrowheads short distances. 20 frames for each molecule in **a**-**l** were collected. One frame per molecule was recorded for the grid translated nanorulers in **m**, **n**. Data in **a**, **b**, **d**, **e**, **g**, and **h** was filtered to a cut-off in localization error of $\sigma_{loc_1} = \sigma_{loc_2} =$ 4.0 nm. Data in **j** and **k** was filtered to a cut-off in localization error of $\sigma_{loc_1} = \sigma_{loc_2} = 6.5$ nm. Single-molecule distances in **a-l** were obtained by selecting time-lapse series of individual molecules (see **Supplementary Table 5**). Details about fitting parameters in **Supplementary Table 3**.

Laser power Ch1 [mW]	Laser power Ch2 [mW]	Exposure time [ms]	Radiant exposure Ch1 [nJ/um^2]	Radiant exposure Ch2 [nJ/um^2]	Noise threshold - beads	Noise threshold - 20 nm ruler	Noise threshold - 30bp dsDNA
0.42	0.38	100	11.75	10.42	100	-	-
0.47	0.41	100	13.03	11.36	200	-	-
0.60	0.51	100	16.53	14.08	300	-	-
0.77	0.65	100	21.42	17.92	400	-	-
1.00	0.82	100	27.67	22.89	800	-	-
1.27	1.05	100	35.39	29.03	1,500	-	-
1.60	1.31	100	44.47	36.31	2,500	-	-
0.84	0.74	400	93.33	82.22	-	220	45
0.84	0.74	800	186.67	164.44	-	400	80
0.84	0.74	1,200	280.00	246.67	-	650	110
0.84	0.74	1,600	373.33	328.89	-	800	150
0.84	0.74	2,000	466.67	411.11	-	1,100	200
3.3	3.0	400	366.7	333.3	-	750	120
3.3	3.0	800	733.3	666.7	-	1,600	250
3.3	3.0	1,200	1,100.0	1,000.0	-	2,250	350
3.3	3.0	1,600	1,466.7	1,333.3	-	2,850	480
3.3	3.0	2,000	1,833.3	1,666.7	-	3,750	600
7.3	6.6	400	811.1	733.3	-	1,650	250
7.3	6.6	800	1,622.2	1,466.7	-	3,300	440
7.3	6.6	1,200	2,433.3	2,200.0	-	4,500	650
7.3	6.6	1,600	3,244.4	2,933.3	-	6,000	820
7.3	6.6	2,000	4,055.6	3,666.7	-	8,000	970
12.7	11.5	400	1,411.1	1,277.8	-	2,100	370
12.7	11.5	800	2,822.2	2,555.6	-	5,500	600

Laser power Ch1 [mW]	Laser power Ch2 [mW]	Exposure time [ms]	Radiant exposure Ch1 [nJ/um^2]	Radiant exposure Ch2 [nJ/um^2]	Noise threshold - beads	Noise threshold - 20 nm ruler	Noise threshold - 30 bp dsDNA
12.7	11.5	1,200	4,233.3	3,833.3	-	8,000	850
12.7	11.5	1,600	5,644.4	5,111.1	-	10,000	1,100
12.7	11.5	2,000	7,055.6	6,388.9	-	12,000	1,400
18.2	16.6	400	2,022.2	1,844.4	-	3,500	400
18.2	16.6	800	4,044.4	3,688.9	-	7,000	750
18.2	16.6	1,200	6,066.7	5,533.3	-	11,000	950
18.2	16.6	1,600	8,088.9	7,377.8	-	13,000	1,250
18.2	16.6	2,000	10,111.1	9,222.2	-	-	1,600
21.6	19.5	400	2,400.0	2,166.7	-	4,300	450
21.6	19.5	800	4,800.0	4,333.3	-	8,800	750
21.6	19.5	1,200	7,200.0	6,500.0	-	12,500	1,000
21.6	19.5	1,600	9,600.0	8,666.7	-	-	1,300
21.6	19.5	2,000	12,000.0	10,833.3	-	-	1,700

Supplementary Table 1 | Calculation of radiant exposures as used in **Supplementary Figure 4**. Laser power was measured at objective. Since we did not have flat field illumination we estimated an area of 60 µm by 60 µm as relative constant to determine radiant exposure. Noise threshold refers to setting in µManger's[1] 'Localization Microscopy' plug-in. It was chosen so that approximately the same number molecules was fitted per micrograph and to avoid fitting background as true particles (especially for higher radiant exposures). More details about fitting parameters in **Supplementary Table 3**.

Laser power Ch1 [mW]	Laser power Ch2 [mW]	Exposure time [ms]	Radiant exposure Ch1 [nJ/um^2]	Radiant exposure Ch2 [nJ/um^2]	Noise threshold - beads	Noise threshold - 20 nm ruler	Noise threshold - 30 bp dsDNA
0.42	0.38	100	11.75	10.42	100	-	-
0.47	0.41	100	13.03	11.36	200	-	-
0.60	0.51	100	16.53	14.08	300	-	-
0.77	0.65	100	21.42	17.92	400	-	-
1.00	0.82	100	27.67	22.89	800	-	-
1.27	1.05	100	35.39	29.03	1,500	-	-
1.60	1.31	100	44.47	36.31	2,500	-	-
0.91	0.77	400	101.33	85.11	-	50	33
1.27	1.05	400	141.00	116.78	-	80	50
1.73	1.40	400	192.00	155.78	-	95	65
2.28	1.86	400	253.33	206.11	-	135	75
2.94	2.42	400	326.78	269.11	-	175	110
3.7	3.1	400	411.1	346.7	-	230	140
4.5	3.8	400	502.2	421.1	-	270	160
5.5	4.7	400	613.3	516.7	-	350	175

Supplementary Table 2 | Calculation of radiant exposures as used in **Supplementary Figure 7**. Laser power was measured at objective. Since we did not have flat field illumination we estimated an area of 60 µm by 60 µm as relative constant to determine radiant exposure. Noise threshold refers to setting in µManger's[1] 'Localization Microscopy' plug-in. It was chosen so that approximately the same number molecules was fitted per micrograph and to avoid fitting background as true particles (especially for higher radiant exposures). More details about fitting parameters in **Supplementary Table 3**.

Imaging Parameters	
Photon conversion factor	1.84
Linear (EM) gain	1.0
Pixel size [nm]	159.0
Time interval [ms]	0.0
Z-step [nm]	50.0
Camera offset [electron counts]	91.0
Read noise [electron counts]	9.84
Find Maxima	
Pre-Filter	None
Noise tolerance	See **Supplementary Table 4**
Fit Parameters	
Dimensions	1
Filter	Simplex-MLE
Max Iterations	500
Box size [pixel]	12.0
Fix width	Not selected
Filter Data	Nothing selected
Positions	Always all, except for registration maps where data is split to create affine and piecewise affine maps so that ~1000 beads can be used for affine map. Remainder is used for piecewise affine map.
Skip Channels	Not selected

Supplementary Table 3 | Fitting parameters used in the μManger's[1] 'Localization Microscopy' plug-in.

Data set in Figure	**Radiant exposure used for sample of interest [nJ/um²]**		**Noise threshold used for sample of interest**
	Channel 1	**Channel 2**	
Fiducials to create *all maps*	35.39	29.03	300
Figure 3	35.39	29.03	300
Figure 4	613.3	516.7	300
Figure 5	613.3	516.7	300
Supplementary Figure 4	See **Supplementary Table 1**		See **Supplementary Table 1**
Supplementary Figure 5	30bp dsDNA: 613.3 20 nm ruler: 613.3 Beads: 35.39	30bp dsDNA: 516.7 20 nm ruler: 516.7 Beads: 29.03	All data sets: 300
Supplementary Figure 7	See **Supplementary Table 2**		See **Supplementary Table 2**
Supplementary Figure 8	35.39	29.03	300
Supplementary Figure 10	35.39	29.03	300
Supplementary Figure 11	35.39	29.03	300
Supplementary Figure 12	a-f: 2,400.0 g-l: 613.3	a-f: 2,166.7 g-l: 516.7	a-f: 300 g-l: 100
Supplementary Figure 13	35.39	29.03	300
Supplementary Figure 14	35.39	29.03	300
Supplementary Figure 15	613.3	516.7	300
Supplementary Figure 16	613.3	516.7	a, b: 3000 c-e: 300
Supplementary Figure 17	141.00	116.78	100
Supplementary Figure 19	a-l: 613.3 m, n: 35.39	a-l: 516.7 m, n: 29.03	a-l: 300 m, n: 300

Supplementary Table 4 | Radiant exposures used for the acquisition of different data sets if not specified elsewhere. Noise tolerance as used in the μManger's[1] 'Localization Microscopy' plug-in for different data sets if not specified elsewhere.

Data set in Figure	Minimum # of Frames	Maximum # of missing Frames	Maximum Distance [nm]	Minimum total distance [nm]	Combine tracks from all channels	Maximum pair distance [nm]
Figure 4	5	15	15	0	Checked	30
Figure 5	15	5	20	0	Checked	c,e: 40 d,f: 60
Supplementary Figure 7	60	10	90	0	Unchecked	-
Supplementary Figure 14	a-f: 3 g-l: 3	a-f: 17 g-l: 17	a-f: 20 g-l: 10	a-f: 0 g-l: 0	a-f: Checked g-l: Checked	a-f: 20 g-l: 20
Supplementary Figure 15	5	15	15	0	Checked	100
Supplementary Figure 16	15	5	20	0	Checked	40
Supplementary Figure 19	a, b: 3 d, e: 3 g, h: 3 j, k: 3 c, f, i, l: 15	a, b: 17 d, e: 17 g, h: 17 j, k: 17 c, f, i, l: 5	a, b: 60 d, e: 60 g, h: 60 j, k: 60 c, f, i, l: 60	a, b: 0 d, e: 0 g, h: 0 j, k: 0 c, f, i, l: 0	all: Checked	a, b, c: 50 d, e, f: 80 g, h, i: 100 j, k, l: 60

Supplementary Table 5 | Settings for the 'Extract Tracks' function in the μManger's[1] 'Localization Microscopy' plug-in used to extract tracks of single-molecules that were imaged for F number of frames. Here maximum distance refers to distance between the position of one molecule from channel n-1 to channel n. Minimum total distance means distance of one molecules' position in frame 1 to its position in frame F. And maximum pair distance selects molecules in which the distance between channel 1 and channel 2 position is below a defined threshold.

Supplementary Note 1

The two-dimensional probability distribution[14] is given by

$$p_{2D}(r) = \left(\frac{r}{\sigma_d{}^2}\right) exp\left(-\frac{\mu^2+r^2}{2\sigma_d{}^2}\right) I_0\left(\frac{r\mu}{\sigma_d{}^2}\right) \tag{1}$$

in which r is the measured Euclidean distance, μ the calculated distance, σ_d the distance uncertainty, and I_0 the modified Bessel function of integer order zero. For $\sigma_d \gg \mu$, r similar order or less than σ_d, and with

$$I_0(z) = \sum_{k=0}^{\infty} \frac{\left(\frac{1}{4}z^2\right)^k}{(k!)^2} \tag{2}$$

we can find the following approximation:

$$p_{2D}(r) \approx \left(\frac{r}{\sigma_d{}^2}\right) exp\left(-\frac{\mu^2+r^2}{2\sigma_d{}^2}\right)\left(1 + \frac{r^2\mu^2}{4\sigma_d{}^4} + ...\right) \tag{3}$$

$$\approx \left(\frac{r}{\sigma_d{}^2}\right) exp\left(-\frac{r^2}{2\sigma_d{}^2}\right)\left(1 - \frac{\mu^2}{2\sigma_d{}^2} + ...\right)\left(1 + \frac{r^2\mu^2}{4\sigma_d{}^4}\right) \tag{4}$$

$$\approx \left(\frac{r}{\sigma_d{}^2}\right) exp\left(-\frac{r^2}{2\sigma_d{}^2}\right)\left(1 + \frac{\mu^2}{2\sigma_d{}^2}\left(\frac{r^2}{2\sigma_d{}^2} - 1\right)\right) \tag{5}$$

$$\approx \left(\frac{r}{\sigma_d{}^2}\right) exp\left(-\frac{r^2}{2\sigma_d{}^2}\right) \tag{6}$$

Thus, the approximation for $\sigma_d \gg \mu$ of the probability distribution (Eq. 2) is independent of μ.

Supplementary Note 2

Predicted and measured localization errors correlate well

When comparing measured and predicted localization errors we realized that they correlate well ($R^2 \geq 0.8$) at low radiant exposures but poorly at high radiant exposures (**Supplementary Fig. 7 h, i**). One explanation for this is that sample imperfections are only revealed at higher radiant exposures (**Supplementary Fig. 7)**. To test this further we performed Avg-Sigma-P2D on single-molecules from the same data set (**Supplementary Fig. 7 j-r**) and noticed that the discrepancy between measured and predicted localization errors for samples with few fluorophores at high radiant exposures is mainly due to intersample distance changes (instability) during measurements (**Supplementary Fig. 7 p-r**). Hence, outliers for which the predicted and measured localization errors do not match are likely caused by sample imperfections.

Supplementary Note 3

Color centers of TetraSpeck beads do not overlap

For TetraSpeck beads the registration precision (σ_x, σ_y) is worse than one would expect based on their localization errors σ_l (σ_{loc_1}, σ_{loc_2} and their standard deviations $\sigma_{\sigma(loc_1)}$, $\sigma_{\sigma(loc_2)}$) (**Supplementary Fig. 12**). To asses if this discrepancy is due to our image registration process or an intrinsic parameter of the beads, we imaged individual beads translated in a 30x30 grid pattern and noticed that most beads have a consistent x-y-distance offset, independent of the position in the image (**Supplementary Fig. 13 a-c**). In an area where grids of two beads overlap we observed that the offset in x and y was a function of the individual bead, not the position in the image (**Supplementary Fig. 13 d-f**). As reported by others[15,16], the offset is likely caused by beads for which the color centers of the two dyes do not exactly overlap but differ by a few nanometers. To test if the registration precision can solely be explained by localization errors σ_l of the test sample we turned to a single biotinylated Cy3/Cy5 dsDNA construct, which has been shown to have no distance variation across molecules and to be of zero distance[15]. Using both, low and high radiant exposures, we found a very good agreement between σ_x and σ_l as well as σ_y and σ_l (**Supplementary Fig. 14**). Thus, these experiments suggest that the sample's localization error σ_l can almost solely account for the registration precision (σ_x, σ_y) as long as the sample is homogenous and registration accuracy is high (< 1 nm).

Supplementary Note 4

The end-to-end distance of many nucleotide based rulers is heterogenous

Because of the variance in distance we observed for proteins, we decided to utilize DNA based rulers to further evaluated Avg-Sigma-P2D and Vector-P2D. We imaged DNA origami nanorulers[17] labeled with multiple dyes of two different spectra and center-of-mass distances of 10 nm, 20 nm, and 40 nm. In addition, we determined the end-to-end distance of a 30 bp dsDNA construct (~10 nm) labeled with Cy3 and Cy5[18]. For all four samples we noticed that only Vector-P2D yielded distances as predicted for ensemble measurements and that Avg-Sigma-P2D only fit well to distance distributions of individual particles suggesting heterogeneity in color center distances (**Supplementary Fig. 19**). This heterogeneity of nanorulers is likely caused by photobleaching and labeling inefficiency resulting in center-of-mass shifts between the dyes (**Supplementary Fig. 7 q, r**). For the 30 bp dsDNA construct the heterogeneity may be caused by hydrophobic or stacking effects of fluorescent probes, often resulting in an anisotropic PSF and systematic localization errors on the order of tens of nanometers[15,16,19,20]. Taken together, these DNA based rulers are heterogeneous with respect to their color center distance (as detected by Avg-Sigma-P2D) and their color center ensemble distance can be correctly determined by Vector-P2D.

Supplementary Protocol

In the following sections we provide a detailed protocol for data acquisition, fitting of emitters, image registration, and data analysis (distance determination) in μManager[1] 2.0. In addition, we provide screenshots of the relevant plugins.

a) Data acquisition

1. Data is acquired in the order as depicted in **Figure 3 a** and as described in the **Online Methods**. For all data collections we used the 'Multi-Dimensional Acquisition' plugin. A detailed manual for data acquisition can be found here. Thus, we will only describe the grid acquisition that we used for the fiducial markers.
2. For the fiducial markers that will be used to create the affine and piecewise affine map as well as the fiducials that will be used to test the map and that are acquired after the sample of interest, select 'Multiple Positions', 'Channels' and 'Save Data' in the 'Multi-Dimensional Acquisition' plugin. Then, click on 'Edit Position List'. A new window 'Stage Position List' will appear.

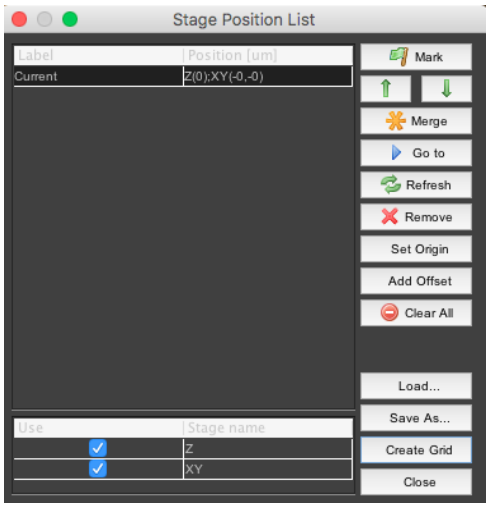

3. In case there are entries in the table, click 'Clear All' first. Then click 'Create Grid'. An additional window 'Tile Creator' will open. By clicking '+' and '-' you can increase or decrease the grid size, respectively. Typically you want to create a 20x20 grid. Afterwards type the overlap size and provide the pixel size. We used an overlap of 71 μm for a micrograph of 81x81 μm. Next, click 'Center Here' and then 'OK'.

4. In the ‘Stage Position List’ window all generated positions for your grid will be listed in the table. If everything looks good, click ‘Close’.
5. For how to change ‘Channel’ and ‘Save Data’ settings see here. Once everything is set, click ‘Acquire!’.

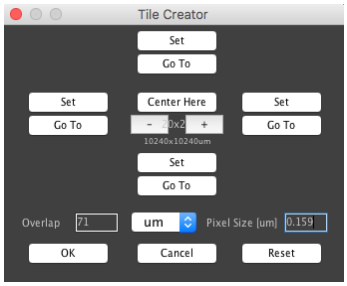

b) Fitting of emitters

6. Open the data with the fiducial markers that were acquired **prior** to the sample of interest by either dragging and dropping the file into µManager or by ‘File’ → ‘Open (RAM)’.
7. Open the ‘Localization Microscopy’ plugin: “Plugins’ → ‘Acquisition Tools’ → ‘Localization Microscopy’ that looks like the one on the right.
8. Provide the ‘Imaging parameters’ that match your settings. For the ‘Find Maxima’ you can use the ‘show’ button to see which particles will get selected with the corresponding ‘Noise tolerance’. For the ‘Fit Parameters’ you want ‘Dimensions’ to be ‘1’, and use the ‘Simplex MLE’ ‘Filter’. We always used ‘500’ as ‘Max Iterations’. For the ‘Box Size’ make sure that you do not select one that is too small because this will overestimate the background. Typically the box size is right, when the localization error does not change anymore when you increase the box size. You can ‘Filter Data’ to remove outliers (optional). If you run any of the example data sets that we provided, use the values as listed in **Supplementary Table 3**.
9. In ‘Positions’ (Positions of your grid (e.g. you may have acquired a 20x20 grid and thus 400 images total)) start with ‘1-20’ and adjust so that you get approximately 1000 spots to create your affine map. Therefore click ‘Fit’. A new window ‘Gaussian tracking data’ will open (see below). The number of spots will be listed in the third column.
10. Use the remaining positions (e.g. ‘21-400’) and click ‘Fit’ again. These fiducial markers will be used to create the piecewise affine map.

11. Open the data with the fiducial markers that were acquired **after** to the sample of interest as described in step 6. This data can be used to test your map (determine the TRE as described in **Online Methods**).
12. Set ‘Positions’ to ‘1-400’ if you acquired a 20x20 grid and click ‘Fit’.
13. Now open a movie/image with the sample of interest as described in step 6. In the ‘Localization Microscopy’ plugin you may want to adjust the ‘Noise Threshold’. Moreover, change ‘Positions’ to ‘1’ since you likely either acquired only a single image or a timelapse movie and did not move to other positions. The click ‘Fit’.
14. Repeat step 13 for all movies with your sample of interest.

b) Image registration

15. Select the data that you want to use for your affine map (typically the data of fiducials that you fitted in step 9 by clicking on the corresponding row.
16. In ‘2-Color’ select ‘Affine’ from the drop-down menu and use a radius of 2000 nm. Then click ‘2C Reference’.
17. Select all other data including fiducials that will be used as your piecewise affine map, and to test your map as well as all data sets with your sample of interest. Then click ‘Correct’ in ‘2-Color’. This will create new files (rows) with the affine corrected data.
18. Now select the affine corrected version of your data that will be used as the piecewise affine map. Often the maps will have a few fiducials that have a very different two-color distances than most others and might throw off the map. To remove those create a custom script. In the general μManager menu go to ‘Tools’ → ‘Script Panel’. In the ‘Script Panel’ click ‘New’. Copy and paste the following script:

    ```
    import edu.ucsf.valelab.gaussianfit.DataCollectionForm;
    dcf = DataCollectionForm.getInstance();
    dcf.filterPairs(50, 2.0, 36);
    ```

    Then click ‘Run’. This will create a new row with data which is your affine corrected and outlier removed data set that will be used as the piecewise affine map.
19. Then select the data created in step 18 and chose ‘Piecewise Affine’ from the ‘2-Color’ drop-down menu and a radius of 100 nm (unless you want measure distances significantly larger than 100 nm, then you want to set it approximately three fold higher than the expected average distance). Then click ‘2C Reference’.

20. Now you want to set the parameters (Minimum and maximum number of fiducials, Maximum distance) for the piecewise affine map. Since we learnt that ‘10’ is the ideal number as minimum points, this value can not be changed. However, the maximum number (currently ‘100’) and maximum distance (currently ‘2000’) can be adjusted. Therefore create another custom script:

    import edu.ucsf.valelab.gaussianfit.DataCollectionForm;

    dcf = DataCollectionForm.getInstance();

    dcf.setPieceWiseAffineParameters(100, 2000);

    Click ‘Run’.

21. Next, select the affine corrected versions of the fiducial data that will be used to test the map and all affine corrected data of your sample of interest. Then click ‘2C Correct’. This command will finally piecewise affine correct all your data.
22. At this point you may find it useful to save your data. Therefore select all rows that you want to save as individual ‘.txt’ files. Then select ‘Text’ and click ‘Save’ in ‘General’ in the ‘Gaussian tracking data’ window. In case you want to load data, you can either click ‘Load’ or drag ‘n drop the ‘.txt’ files into the ‘Gaussian tracking data’ window.
23. In case you want to filter any of your files by number of photons (Intensity) or localization error (Sigma), select the corresponding rows. Then type the desired values in ‘Filters’ in the ‘Gaussian tracking data’ window and click ‘Filter Now’. As before, this will create new data/rows with your filtered data sets.

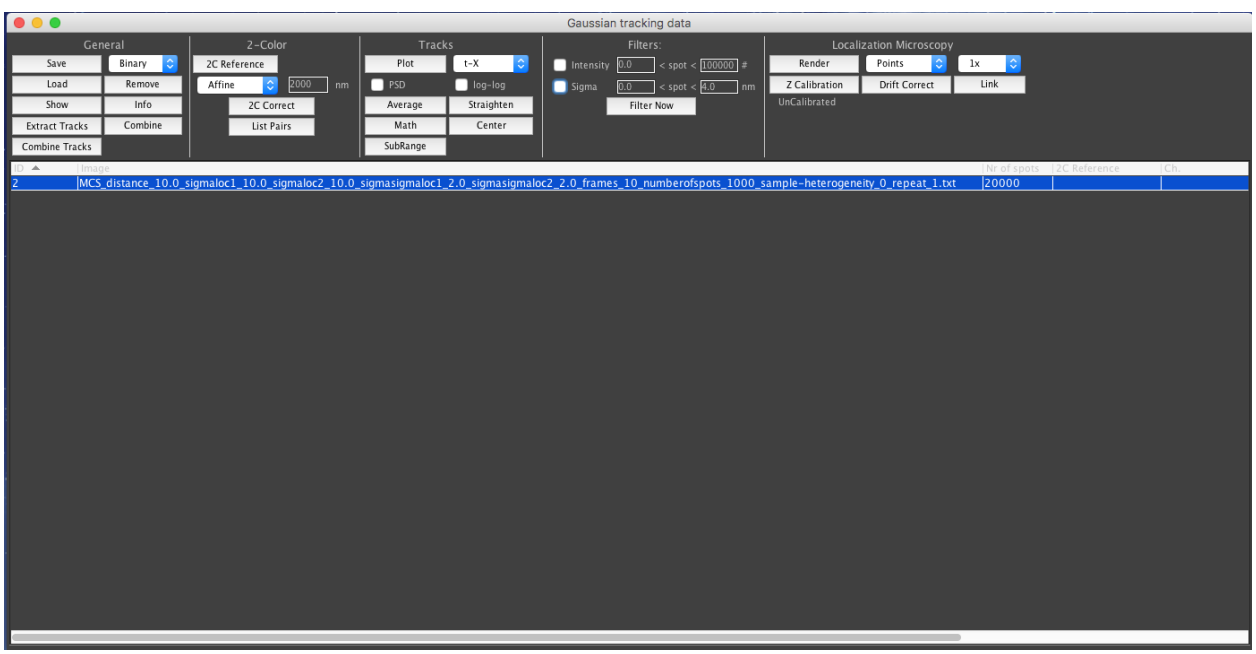

d) Data analysis and distance determination

24. If you have more than one movie/image of your sample of interest, you may want to combine all of them now. Therefore select all files/rows and click 'Combine' in 'General' in the 'Gaussian tracking data' window. This will create a data set/row with all files combined. However, when files get combined they still keep unique identifiers. In this case different movies will be assigned different positions. You can see this by selecting the file with the combined data and by clicking 'Show'. This will open a window with all relevant values like frame number, channel, position, intensity (# of photons), and sigma (localization error). Note, this is the exact same data, that gets saved, when you click 'Save'.

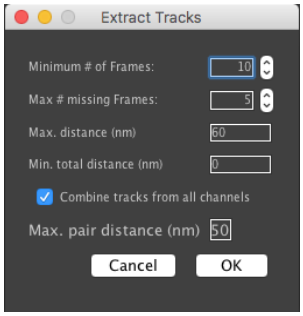

25. This step is optional and only required if you want to extract tracks with defined parameters (remove outliers). A 'Track' here refers to the data (localizations) of the same spot that was imaged over multiple times (timelapse). Thus, if you acquired a single image only, you should skip this step.
    Select either individual files of your data of interest or the combined version as created in step 24. Then click 'Extract Tracks'. This will open a window as shown above. Here is what each of the settings mean:
    - 'Minimum # of frames': Say you acquired movies with 20 frames, then you may want to select only spots that have more than 15 frames total to remove spots that bleached earlier or that blinked a lot.
    - 'Max # of missing Frames': Define how many frames can be missing (due to blinking) between the first and last localization.
    - 'Max distance (nm)': This determines how far localization n can be away from localization n-1 (e.g. it should not jump by 1000 nm).
    - 'Min total distance (nm)': Irrelevant here. Set to '0'.
    - 'Combine tracks from channels': If selected, it will combine tracks from channel 1 and 2 which have localizations in at least one and the same frame that are less than 'Max. pair distances (nm)' apart.
    - 'Max. pair distances (nm)': See 'Combine tracks from channels'.

    Select your values. If you run any of the example data that we provided, use the values as listed in **Supplementary Table 5**. Then click 'OK'. This will create new rows for each

track. Typically you will only care about tracks that have both, channel 1 and 2. These will be listed in the fifth column in the table of the 'Gaussian tracking data' window as '1,2'. Now, you can combine all tracks that have both channels by selecting these and by clicking 'Combine' (similar to step 24).

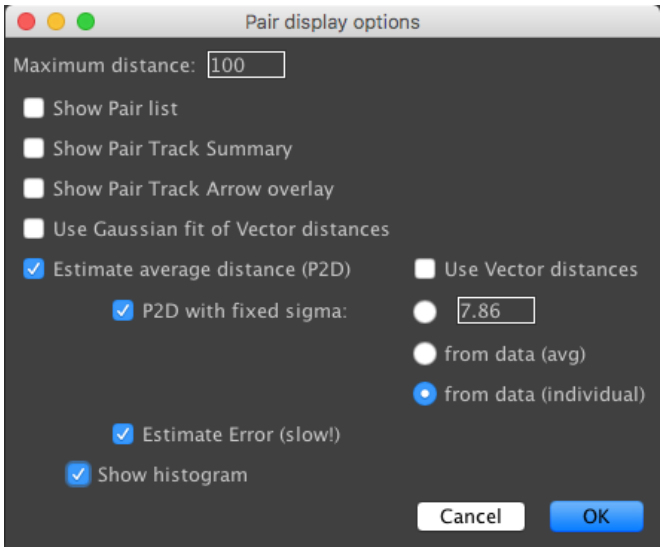

26. Now, you can determine the distance. Select either data as combined in step 24, or the 'Extract Tracks' purified data from step 25, or individual tracks of a single-molecule that you created in step 25. Then click 'List Pairs' and a new window ('Pair display options') will open. Here you have various options which will be discussed below (all can be executed at the same time):
    - 'Maximum distance': Provide the cutoff for the maximum distance of a dye pair. This should not be larger than the value you used for the piecewise affine map in step 19.
    - 'Show Pair list': If selected, this will open a window with values like all pairwise distances, position, frame number, and localization errors of individual dye pairs. You can save this table by right click → 'Save As...'.
    - 'Show Pair Track Summary': Can only be used if more than one frame per position was acquired (movie but not single image). If selected, this will open a window with values of all frame-by-frame distance averages and their standard deviation, vector distance averages and their standard deviations, number of frames, localization errors, and more. You can save this table by right click → 'Save As...'.
    - 'Show Pair Track Arrow Overlay': Draws arrows into the micrograph to show orientation and magnitude of distance of individual pairwise distances. By orientations we mean an arrow pointing from channel 1 to channel 2. This can be useful to quickly evaluate if the registration map creates larger, correlated

patches when plotting the arrows for the corrected fiducial markers that were acquired after the sample of interest.

- ‘Use Gaussian fit of Vector Distances’: This will open a window with a histogram of vector averaged distances and a Gaussian fit on top of it (Vector). You can save this figure by right click → ‘Save As...’.
- ‘Estimate average distance (P2D)’: This function has multiple subcategories and will calculate distances with the corresponding fit:
  i. ‘Use Vector distances’: executes Vector-P2D
  ii. If just ‘Estimate average distance (P2D)’ is selected and nothing else, a Churchman-P2D fit[14] will be performed.
  iii. ‘P2D with fixed sigma’:
     a. ‘Textfield’: Hard code your own value that should be used as σ_d in equation 2.
     b. ‘from data (avg)’: Calculates σ_d as in equation 1 to be used in equation 2 (Avg-Sigma-P2D).
     c. ‘from data (individual)’: Calculates σ_d for individual spot pairs to be used in equation 2.
  iv. ‘Estimate Error’: Calculates an error for the predicted distance by means of bootstrapping.
  v. ‘Show histogram’: Will plot a histogram with the distance distribution and the selected fit(s). This can be saved as a ‘.png’ by right click → ‘Save as …’

Supplementary References

1. Edelstein, A., Amodaj, N., Hoover, K., Vale, R. & Stuurman, N. Computer control of microscopes using μManager. *Curr. Protoc. Mol. Biol.* **Chapter 14,** Unit14.20 (2010).
2. Thompson, R. E., Larson, D. R. & Webb, W. W. Precise nanometer localization analysis for individual fluorescent probes. *Biophys. J.* **82,** 2775–2783 (2002).
3. Mortensen, K. I., Churchman, L. S., Spudich, J. A. & Flyvbjerg, H. Optimized localization analysis for single-molecule tracking and super-resolution microscopy. *Nat. Methods* **7,** 377–381 (2010).
4. Endesfelder, U., Malkusch, S., Fricke, F. & Heilemann, M. A simple method to estimate the average localization precision of a single-molecule localization microscopy experiment. *Histochem. Cell Biol.* **141,** 629–638 (2014).
5. Ober, R. J., Ram, S. & Ward, E. S. Localization accuracy in single-molecule microscopy. *Biophys. J.* **86,** 1185–1200 (2004).
6. Fitzpatrick, J. M. Fiducial registration error and target registration error are uncorrelated. in *Proc SPIE* **7261,** 726102–726112 (2009).
7. Keppler, A. *et al.* A general method for the covalent labeling of fusion proteins with small molecules in vivo. *Nat. Biotechnol.* **21,** 86–89 (2003).
8. Los, G. V. *et al.* HaloTag: a novel protein labeling technology for cell imaging and protein analysis. *ACS Chem. Biol.* **3,** 373–382 (2008).
9. Liu, Y. *et al.* Bicaudal-D uses a parallel, homodimeric coiled coil with heterotypic registry to coordinate recruitment of cargos to dynein. *Genes Dev.* **27,** 1233–1246 (2013).
10. Mollwitz, B. *et al.* Directed evolution of the suicide protein O 6-alkylguanine-DNA alkyltransferase for increased reactivity results in an alkylated protein with exceptional

stability. *Biochemistry* **51,** 986–994 (2012).

11. Liu, Y. *et al.* The Cation-π Interaction Enables a Halo-Tag Fluorogenic Probe for Fast No-Wash Live Cell Imaging and Gel-Free Protein Quantification. *Biochemistry* **56,** 1585–1595 (2017).
12. Pettersen, E. F. *et al.* UCSF Chimera—A visualization system for exploratory research and analysis. *J. Comput. Chem.* **25,** 1605–1612 (2004).
13. Alva, V., Nam, S.-Z., Söding, J. & Lupas, A. N. The MPI bioinformatics Toolkit as an integrative platform for advanced protein sequence and structure analysis. *Nucleic Acids Res.* **44,** W410–5 (2016).
14. Churchman, L. S., Flyvbjerg, H. & Spudich, J. A. A non-Gaussian distribution quantifies distances measured with fluorescence localization techniques. *Biophys. J.* **90,** 668–671 (2006).
15. Pertsinidis, A., Zhang, Y. & Chu, S. Subnanometre single-molecule localization, registration and distance measurements. *Nature* **466,** 647–651 (2010).
16. Mortensen, K. I., Sung, J., Flyvbjerg, H. & Spudich, J. A. Optimized measurements of separations and angles between intra-molecular fluorescent markers. *Nat. Commun.* **6,** 8621 (2015).
17. Schmied, J. J. *et al.* DNA origami-based standards for quantitative fluorescence microscopy. *Nat. Protoc.* **9,** 1367–1391 (2014).
18. Churchman, L. S., Okten, Z., Rock, R. S., Dawson, J. F. & Spudich, J. A. Single molecule high-resolution colocalization of Cy3 and Cy5 attached to macromolecules measures intramolecular distances through time. *Proc. Natl. Acad. Sci. U. S. A.* **102,** 1419–1423 (2005).
19. Enderlein, J., Toprak, E. & Selvin, P. R. Polarization effect on position accuracy of

fluorophore localization. *Opt. Express* **14,** 8111–8120 (2006).

20. Stallinga, S. & Rieger, B. Accuracy of the gaussian point spread function model in 2D localization microscopy. *Opt. Express* **18,** 24461–24476 (2010).